# Carbonylation Chemistry of the Tantalum Silyl $(\eta^5\text{-}C_5Me_5)Cl_3TaSiMe_3$. Synthesis, Characterization, and Reaction Chemistry of $(\eta^5\text{-}C_5Me_5)Cl_3Ta(\eta^2\text{-}COSiMe_3)$ and Derivatives

**John Arnold,[†] T. Don Tilley,*[,†] Arnold L. Rheingold,*[,‡] Steven J. Geib,[‡] and Atta M. Arif[§]**

*Contribution from the Chemistry Department, D-006, University of California at San Diego, La Jolla, California 92093, the Department of Chemistry, University of Delaware, Newark, Delaware 19716, and the Department of Chemistry, The University of Texas at Austin, Austin, Texas 78712.* *Received April 18, 1988*

**Abstract:** The carbonylation chemistry of $(\eta^5\text{-}C_5Me_5)Cl_3TaSiMe_3$ (**1**) is described in detail. With limited quantities of carbon monoxide, **1** is converted to the thermally unstable $\eta^2$-silaacyl $(\eta^5\text{-}C_5Me_5)Cl_3Ta(\eta^2\text{-}COSiMe_3)$ (**2**). Compound **2** was characterized spectroscopically. The electrophilic behavior of **2** is demonstrated by its reactions with simple Lewis bases. These reactions provide the adducts $(\eta^5\text{-}C_5Me_5)Cl_3Ta[\eta^2\text{-}OC(L)(SiMe_3)]$, where L is pyridine (**3**), 2,6-dimethylpyridine (**4**), $PMe_3$ (**5**), and $PEt_3$ (**6**). The lability of these complexes in solution is described. Diphenyldiazomethane forms an adduct with **2**, $(\eta^5\text{-}C_5Me_5)Cl_3Ta[OC(SiMe_3)NNCPh_2]$ (**8**), that does not contain a Ta–C(acyl) bond and possesses a benzophenone silaacylhydrazonato ligand. Pyridine reacts with the phosphine adducts **5** and **6** to give a product in which the silaacyl carbon has inserted into the ortho C–H bond of pyridine, $(\eta^5\text{-}C_5Me_5)Cl_3Ta[OCH(SiMe_3)\text{-}o\text{-}C_5H_4N]$ (**10**). The tungsten dihydride $(\eta^5\text{-}C_5H_5)_2WH_2$ apparently adds to the carbonyl group of **2**, and subsequent rearrangements yield $(\eta^5\text{-}C_5H_5)_2W(CH_2SiMe_3)Cl$ (**11**) and $[(\eta^5\text{-}C_5Me_5)Cl_2TaO]_n$ (**12**). In the presence of excess CO, **2** undergoes carbon–carbon coupling to generate a reactive, ketene-like species. This intermediate cleaves ethers containing $\beta$-hydrogens, affording alkoxy ester derivatives of the type $(\eta^5\text{-}C_5Me_5)Cl_3Ta[OCH(SiMe_3)C(O)OR]$. Thus, in diethyl ether the ether-cleavage products **13** (R = Et) and $CH_2{=}CH_2$ are obtained. In 2-methyltetrahydrofuran, complex **15** (R = $(CH_2)_3CH{=}CH_2$) is produced. In tetrahydrofuran, ether cleavage is not observed. Instead, the tantalum(III) product $(\eta^5\text{-}C_5Me_5)Cl_2Ta(CO)_2(THF)$ (**16**) and $Me_3SiCl$ are obtained via an apparent ligand-induced reductive elimination. The THF in **16** is displaced by $PMe_3$, providing purple $(\eta^5\text{-}C_5Me_5)Cl_2Ta(CO)_2(PMe_3)$ (**17**). The ketene-like intermediate is trapped with 2,6-dimethylpyridine (DMP) or tricyclohexylphosphine ($PCy_3$) to give the ylide complexes $(\eta^5\text{-}C_5Me_5)Cl_3Ta[OC(SiMe_3)C(L)O]$ (**18**, L = DMP; **19**, L = $PCy_3$). The related chemistry of $(\eta^5\text{-}C_5Me_5)Cl_3Ta(\eta^2\text{-}COCH_2CMe_3)$ (**21**), obtained from $(\eta^5\text{-}C_5Me_5)Cl_3TaCH_2CMe_3$ (**20**) and CO, has been briefly examined. Compound **21** reacts with pyridine to afford the complex $(\eta^5\text{-}C_5Me_5)Cl_3Ta(\eta^2\text{-}COCH_2CMe_3)(pyr)$, characterized by low-temperature NMR spectroscopy. No complexation of pyridine to the $\eta^2$-acyl ligand of **21** was observed. Extended reaction between **21** and pyridine at room temperature results in a 1,2-hydrogen shift that affords $(\eta^5\text{-}C_5Me_5)Cl_3Ta(cis\text{-}OCH{=}CHCMe_3)(pyr)$ (**23**). The mechanisms of the above transformations are discussed. The molecular structures of complexes **3**, **6**, and **19** are also reported. Crystals of **3** are monoclinic, $P2_1/n$, with $a$ = 10.322 (2) Å, $b$ = 14.503 (3) Å, $c$ = 16.289 (3) Å, $\beta$ = 101.73 (1)°, $V$ = 2392.2 (7) Å$^3$, $Z$ = 4, $R_F$ = 2.62%, and $R_{wF}$ = 2.72%. Crystals of **6** are orthorhombic, $Pcam$, with $a$ = 15.820 (4) Å, $b$ = 11.314 (4) Å, $c$ = 14.809 (5) Å, $V$ = 2651 (1) Å$^3$, $Z$ = 4, $R_F$ = 6.77%, and $R_{wF}$ = 8.06%. The asymmetric unit consists of two half-occupancy molecules intertwined about a mirror plane. Crystals of **19** are monoclinic, $P2_1/n$, with $a$ = 14.751 (2) Å, $b$ = 16.294 (3) Å, $c$ = 16.378 (4) Å, $\beta$ = 105.81 (2)°, $V$ = 3787 (1) Å$^3$, $Z$ = 4, $R_F$ = 6.41%, and $R_{wF}$ = 7.48%.

The potent reactivity of early transition metal,[1] lanthanide,[2] and actinide[3] alkyl derivatives toward carbon monoxide has led to numerous theoretical and experimental investigations. The $\eta^2$-acyl complexes that result from this reactivity have also generated wide interest, particularly with regard to their electrophilicity, which has been ascribed to carbene[1a,3a] or carbenium ion[1b] character at the acyl carbon atom. This characteristic is expressed in a variety of ways, as in the migration of an alkyl[1f,4] or hydride[4b,5] ligand to the $\eta^2$-acyl, with ketone or aldehyde formation. Similar reactions that afford bimetallic compounds with bridging organic carbonyl ligands occur intermolecularly, via addition of M–C[6] or M–H[1k,7] bonds to the $\eta^2$-acyl carbon atom. Norton and co-workers have shown that the conversion in eq 1 (Cp = $\eta^5$-$C_5H_5$) involves nucleophilic attack by the molybdenum

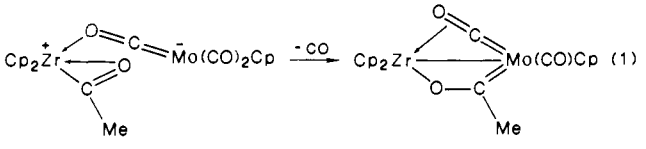

(1)

of the $(\mu\text{-}OC)Mo(CO)_2Cp$ ligand onto the $\eta^2$-acyl carbon, rather than the migration of a carbenoid carbon from zirconium to molybdenum.[6b] Perhaps the most explicit demonstration of the

[†] University of California at San Diego.
[‡] University of Delaware.
[§] The University of Texas at Austin.

(1) Leading references include: (a) Wolczanski, P. T.; Bercaw, J. E. *Acc. Chem. Res.* **1980**, *13*, 121. (b) Tatsumi, K.; Nakamura, A.; Hofmann, P.; Stauffert, P.; Hoffmann, R. *J. Am. Chem. Soc.* **1985**, *107*, 4440. (c) Marsella, J. A.; Moloy, K. G.; Caulton, K. G. *J. Organomet. Chem.* **1980**, *201*, 389. (d) Fachinetti, G.; Fochi, G.; Floriani, C. *J. Chem. Soc., Dalton Trans.* **1977**, 1946. (e) Erker, G. *Acc. Chem. Res.* **1984**, *17*, 103. (f) Bristow, G. S.; Lappert, M. F.; Martin, T. R.; Atwood, J. L.; Hunter, W. F. *J. Chem. Soc., Dalton Trans.* **1984**, 399. (g) Calderazzo, F. *Angew. Chem., Int. Ed. Engl.* **1977**, *16*, 299. (h) Engelhardt, L. M.; Jacobsen, G. E.; Raston, C. L.; White, A. H. *J. Chem. Soc., Chem. Commun.* **1984**, 220. (i) Young, S. J.; Hope, H.; Schore, N. E. *Organometallics* **1984**, *3*, 1585. (j) Fanwick, P. E.; Kobriger, L. M.; McMullen, A. K.; Rothwell, I. P. *J. Am. Chem. Soc.* **1986**, *108*, 8095. (k) Gell, K. I.; Posin, P.; Schwartz, J.; Williams, G. M. *Ibid.* **1982**, *104*, 1846. (l) Klei, E.; Teuben, J. H. *J. Organomet. Chem.* **1981**, *222*, 79. (m) Moore, E. J.; Straus, D. A.; Armantrout, J.; Santarsiero, B. D.; Grubbs, R. H.; Bercaw, J. E. *J. Am. Chem. Soc.* **1983**, *105*, 2068.

(2) (a) Evans, W. J. *Adv. Organomet. Chem.* **1985**, *24*, 131. (b) Evans, W. J.; Wayda, A. L.; Hunter, W. E.; Atwood, J. L. *J. Chem. Soc., Chem. Commun.* **1981**, 706. (c) Evans, W. J.; Hughes, L. A.; Drummond, D. K.; Zhang, H.; Atwood, J. L. *J. Am. Chem. Soc.* **1986**, *108*, 1722.

(3) (a) Moloy, K. G.; Fagan, P. J.; Manriquez, J. M.; Marks, T. J. *J. Am. Chem. Soc.* **1986**, *108*, 56. (b) Sonnenberger, D. C.; Mintz, E. A.; Marks, T. J. *Ibid.* **1984**, *106*, 3484. (c) Moloy, K. G.; Marks, T. J. *Ibid.* **1984**, *106*, 7051. (d) Fagan, P. J.; Manriquez, J. M.; Marks, T. J.; Day, V. W.; Vollmer, S. H.; Day, C. S. *Ibid.* **1980**, *102*, 5393. (e) Marks, T. J. *Science (Washington, D.C.)* **1982**, *217*, 989. (f) Tatsumi, K.; Nakamura, A.; Hofmann, P.; Hoffmann, R.; Moloy, K. G.; Marks, T. J. *J. Am. Chem. Soc.* **1986**, *108*, 4467, and references in the above.

0002-7863/89/1511-0149$01.50/0 

electrophilic character of $\eta^2$-acyl ligands is their formation of adducts with simple Lewis bases, which has now been observed in a few cases. Such reactions have been shown to occur intramolecularly (eq 2[8] and 3[9]) or intermolecularly (eq 4[10] and 5,[11] $Cp^* = \eta^5$-$C_5Me_5$).

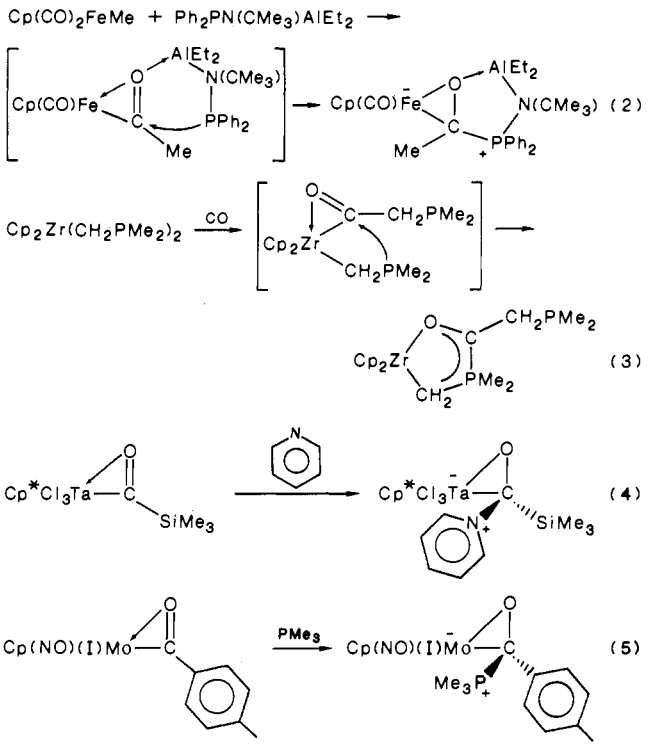


In some cases, carbonylation of formally electron-deficient alkyl complexes results in carbon–carbon bond formation via coupling processes involving intermediate $\eta^2$-acyls. Such processes have afforded monomeric and dimeric *cis*-enediolates,[12] dimeric enedionediolates,[2b,3a] and a monomeric enolate, $[(Me_3Si)_2N]_2Zr[OC(Me)=CMe_2]Me$.[13] Formation of the enedionediolate $\{Cp^*_2Th[OC(CH_2CMe_3)CO]Cl\}_2$ appears to involve coupling of the $\eta^2$-acyl $Cp^*_2Th(\eta^2\text{-}COCH_2CMe_3)Cl$ with carbon monoxide to give a transient, ketene-like species $Cp^*_2Th[OC(CH_2CMe_3)=C=O]Cl$.[3a]

The reactivity of analogous metal–silicon-bonded compounds toward carbon monoxide has not been examined as extensively. Recently, the first example of insertion of CO into a transition metal–silicon bond was reported for a zirconium silyl complex (eq 6).[14] This insertion chemistry has been extended to other early

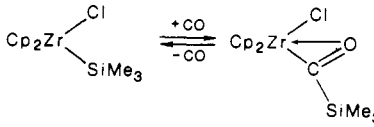


transition metal silyls which readily form $\eta^2$-silaacyl complexes.[15] Although the silaacyl $Cp_2Zr(\eta^2\text{-}COSiMe_3)Cl$ does not react appreciably with simple Lewis bases (including CO), it does combine with the isocyanide $2,6\text{-}Me_2C_6H_3NC$ to form the linear ketenimine $Cp_2Zr[OC(SiMe_3)=C=N(2,6\text{-}Me_2C_6H_3)]Cl$.[15a]

This paper describes the carbonylation chemistry of the electron-deficient (formally 14-electron) tantalum silyl $Cp^*Cl_3TaSiMe_3$ (**1**).[16] These investigations have provided an $\eta^2$-silaacyl complex, $Cp^*Cl_3Ta(\eta^2\text{-}COSiMe_3)$ (**2**), that is quite reactive toward a variety of nucleophilic reagents and cleanly gives a number of stable addition products.

## Results

**Preparation and Properties of $Cp^*Cl_3Ta(\eta^2\text{-}COSiMe_3)$ (2).** Green pentane solutions of **1** slowly turn orange when stirred under an atmosphere of CO at room temperature. If quickly cooled to −45 °C, the $\eta^2$-silaacyl **2** precipitates from solution in good yield as an orange powder. Alternatively, removal of volatiles from the reaction solution affords **2** in slightly less pure form. Traces of **1** are observed by this latter method, indicating that carbonylation of **1** is to some extent reversible (eq 7).

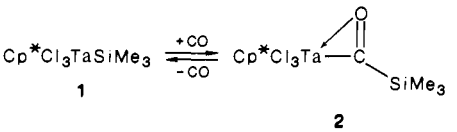


As a solid under argon or nitrogen, **2** decomposes rapidly at room temperature to a complex mixture of products (by $^1H$ NMR) but is stable for at least a week at −45 °C. The decomposition is slower in solution (pentane or benzene) and is dependent on carbon monoxide concentration. In the presence of 1 equiv of CO, **2** is stable for approximately 1 h at 22 °C in benzene-$d_6$. With >3 equiv of CO, decomposition is complete within 30 min by $^1H$ NMR. Attempts to characterize the decomposition products from reaction of **2** with excess CO were unsuccessful, but mixtures of tantalum carbonyl species were detected by infrared spectroscopy.

Complex **2** was characterized by spectroscopic methods and by preparation of derivatives (vide infra). Infrared and NMR data are consistent with those observed for related $\eta^2$-acyls[1-4] and are more similar to values obtained for $Zr(\eta^2\text{-}COSiR_3)$ complexes.[14,15a,e] Solution IR spectra (benzene-$d_6$) for **2** and **2**-$^{13}C$ (prepared from **1** and $^{13}CO$) display $\nu_{CO}$ absorptions at 1462 and 1428 $cm^{-1}$, respectively. Low-temperature $^{13}C$ NMR spectra of **2**-$^{13}C$ exhibit a single, sharp, intense peak at $\delta$ 351 that broadens as the temperature is raised (fwhm = 60 Hz at 22 °C), possibly due to quadrupolar broadening by the $^{181}Ta$ nucleus. In the $^1H$ NMR spectrum of **2**-$^{13}C$, the $SiMe_3$ protons are split into a doublet ($^3J_{CH}$ = 2.4 Hz). Similar $^3J_{CH}$ coupling constants have been observed in $Zr(\eta^2\text{-}^{13}COSiMe_3)$ derivatives.[15a]

(4) (a) Erker, G.; Rosenfeldt, F. *J. Organomet. Chem.* **1982**, *224*, 29. (b) Manriquez, J. M.; McAlister, D. R.; Sanner, R. D.; Bercaw, J. E. *J. Am. Chem. Soc.* **1978**, *100*, 2716. (c) McDermott, J. X.; Wilson, M. E.; Whitesides, G. M. *Ibid.* **1976**, *98*, 6529. (d) Fachinetti, G.; Floriani, C. *J. Chem. Soc., Chem. Commun.* **1972**, 654. (e) Erker, G.; Dorf, U.; Czisch, P.; Petersen, J. L. *Organometallics* **1986**, *5*, 668. (f) Stella, S.; Floriani, C. *J. Chem. Soc., Chem. Commun.* **1986**, 1053. (g) Wood, C. D.; Schrock, R. R. *J. Am. Chem. Soc.* **1979**, *101*, 5421. (h) Erker, G.; Czisch, P.; Schlund, R.; Angermund, K.; Krüger, C. *Angew. Chem., Int. Ed. Engl.* **1986**, *25*, 364.

(5) Roddick, D. M. Ph.D. Thesis, California Institute of Technology, 1984.

(6) (a) Waymouth, R. M.; Clauser, K. R.; Grubbs, R. H. *J. Am. Chem. Soc.* **1986**, *108*, 6385. (b) Martin, B. D.; Matchett, S. A.; Norton, J. R.; Anderson, O. P. *Ibid.* **1985**, *107*, 7952.

(7) (a) Threlkel, R. H.; Bercaw, J. E. *J. Am. Chem. Soc.* **1981**, *103*, 2650. (b) Marsella, J. A.; Folting, K.; Huffman, J. C.; Caulton, K. G. *Ibid.* **1982**, *103*, 5596. (c) Marsella, J. A.; Huffman, J. C.; Caulton, K. G.; Longato, B.; Norton, J. R. *Ibid.* **1982**, *104*, 6360. (d) Gell, K. I.; Williams, G. M.; Schwartz, J. *J. Chem. Soc., Chem. Commun.* **1980**, 550. (e) Marsella, J. A.; Huffman, J. C.; Folting, K.; Caulton, K. G. *Inorg. Chim. Acta* **1985**, *96*, 161. (f) Erker, G.; Kropp, K.; Krüger, C.; Chiang, A.-P. *Chem. Ber.* **1982**, *115*, 2447. (g) Maatta, E. A.; Marks, T. J. *J. Am. Chem. Soc.* **1981**, *103*, 3576. (h) Gambarotta, S.; Floriani, C.; Chiesi-Villa, A.; Guastini, C. *Ibid.* **1983**, *105*, 1690.

(8) Labinger, J. A.; Bonfiglio, J. N.; Grimmett, D. L.; Masuo, S. T.; Shearin, E.; Miller, J. S. *Organometallics* **1983**, *2*, 733.

(9) Karsch, H. H.; Müller, G.; Krüger, C. *J. Organomet. Chem.* **1984**, *273*, 195.

(10) Arnold, J.; Tilley, T. D.; Rheingold, A. L. *J. Am. Chem. Soc.* **1986**, *108*, 5355.

(11) Bonnesen, P. V.; Yau, P. K. L.; Hersh, W. H. *Organometallics* **1987**, *6*, 1587.

(12) See, for example, ref 1a,e, 3f, 4b, and 7g and references therein.

(13) Planalp, R. P.; Andersen, R. A. *J. Am. Chem. Soc.* **1983**, *105*, 7774.

(14) Tilley, T. D. *J. Am. Chem. Soc.* **1985**, *107*, 4084.

(15) (a) Campion, B. K.; Falk, J.; Tilley, T. D. *J. Am. Chem. Soc.* **1987**, *109*, 2049. (b) Arnold, J.; Tilley, T. D. *Ibid.* **1985**, *107*, 6409. (c) Arnold, J.; Tilley, T. D.; Rheingold, A. L.; Geib, S. J. *J. Chem. Soc., Chem. Commun.* **1987**, 793. (d) Arnold, J.; Tilley, T. D.; Rheingold, A. L.; Geib, S. J. *Inorg. Chem.* **1987**, *26*, 2556. (e) Elsner, F. H.; Woo, H.-G.; Tilley, T. D. *J. Am. Chem. Soc.* **1988**, *110*, 313. (f) Arnold, J.; Woo, H.-G.; Tilley, T. D.; Rheingold, A. L.; Geib, S. J. *Organometallics* **1988**, *7*, 2045. (g) Roddick, D. M.; Heyn, R. H.; Tilley, T. D. *Organometallics*, in press.

(16) (a) Arnold, J.; Shina, D. N.; Tilley, T. D.; Arif, A. M. *Organometallics* **1986**, *5*, 2037. (b) Arnold, J.; Tilley, T. D. *J. Am. Chem. Soc.* **1987**, *109*, 3318.

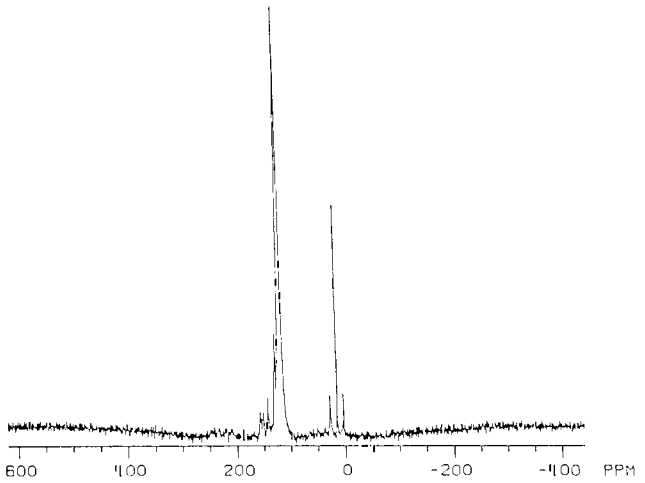


**Figure 1.** $^{13}C$ CP-MAS solid-state NMR spectrum of $Cp^*Cl_3Ta[\eta^2$-$O^{13}C(DMP)SiMe_3]$ (4-$^{13}C$).

**Formation of Silaacyl–Lewis Base Adducts $Cp^*Cl_3Ta[\eta^2$-OC(L)$SiMe_3]$.** Addition of pyridine (≥1 equiv) to a pentane solution of **2** results in immediate precipitation of yellow-orange, microcrystalline $Cp^*Cl_3Ta[\eta^2$-OC(pyr)$SiMe_3]$(**3**) in quantitative yield. Compound **3** is also obtained when pentane solutions of **1** are carbonylated (10–100 psi) in the presence of pyridine (eq 8).

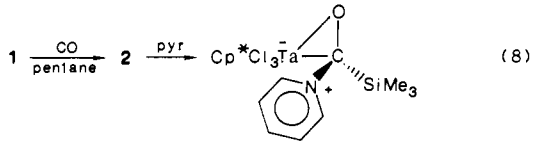


(8)

**3**

Following crystallization from toluene, pure **3** is obtained as small orange prisms in 92% yield. Solid **3** is stable indefinitely under an inert atmosphere at room temperature. Benzene-$d_6$ solutions of **3** remain unchanged after several weeks at room temperature, but if the solutions are heated above ca. 90 °C, decomposition is rapid.

Complex **3** has been characterized by IR and NMR spectroscopy, elemental analysis, and X-ray crystallography (vide infra). The $\nu_{CO}$ stretching frequency (1039 $cm^{-1}$ for **3**, 1022 $cm^{-1}$ for **3**-$^{13}C$) indicates considerable reduction of the C–O bond. For comparison, the analogous stretches in the acetone complex $Cp^*Me_2Ta(\eta^2$-$OCMe_2)$ are at 1200 and 1180 $cm^{-1}$, respectively.[4g] Coordination of pyridine to the silaacyl ligand results in a dramatic upfield shift of the silaacyl carbon resonance, from δ 351 for **2**-$^{13}C$ to δ 117.2 for **3**-$^{13}C$. On the NMR time scale, rotation about the C(acyl)–N(pyridine) bond is slow. Thus, the pyridine in **3** exhibits five distinct signals in $^1$H and $^{13}C$ NMR spectra from −75 to +90 °C.

A 2,6-dimethylpyridine (DMP) adduct of **2** precipitates from pentane in a reaction similar to that used to prepare **3** (eq 9).

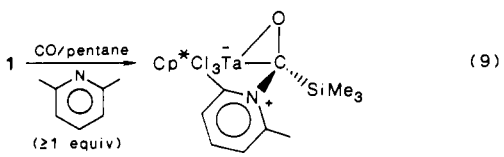


(9)

**4**

Orange, microcrystalline **4** is stable indefinitely under an inert atmosphere but is unstable in solution. On dissolution in benzene-$d_6$ a homogeneous pale green solution is formed, containing **2** (0.9 equiv), **1** (trace), free DMP (1 equiv), and traces of decomposition products (by $^1$H NMR). These results are consistent with extensive dissociation of DMP in solution and the equilibria of eq 10. Similarly, by $^{13}C$ NMR (with **4**-$^{13}C$ in toluene-$d_8$), the only peaks derived from $^{13}CO$ were those due to **2** and free $^{13}CO$. No evidence was found for adduct formation in solution down to

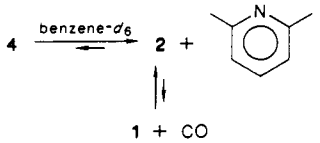


(10)

−70 °C by $^1$H or $^{13}C$ NMR. Since characterization of this exceedingly weak adduct was impossible by solution NMR, solid-state characterization techniques were employed. The infrared spectrum of a Nujol mull of **4** exhibits features similar to those of the pyridine adduct **3**. In addition to resonances for Cp*, $SiMe_3$, and DMP ligands, the $^{13}C$ CP-MAS solid-state NMR spectrum of **4**-$^{13}C$ (Figure 1) shows a broad, intense singlet at δ 117 (fwhm = 180 Hz). This feature is assigned to the $^{13}C$ atom of the DMP-complexed silaacyl ligand in **4**-$^{13}C$.

The phosphane adducts $Cp^*Cl_3Ta[\eta^2$-$OC(PR_3)SiMe_3]$ (**5**, R = Me; **6**, R = Et; **7**, R = OMe[15d]) were prepared in a manner analogous to the pyridine derivatives **3** and **4** (eq 11). In these

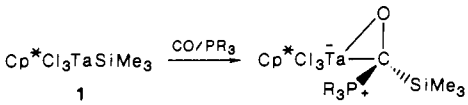


(11)

**5**, R = Me
**6**, R = Et
**7**, R = OMe

reactions, the trivalent phosphorus donor traps the silaacyl **2** as it is formed. Adducts **5** and **6** precipitate from pentane as orange powders in high yield and are stable as solids for an indefinite period under nitrogen. Attempts to obtain analytically pure samples of **5** and **6** by recrystallization were thwarted by decomposition—these complexes were, therefore, characterized by NMR and IR spectroscopy. Additionally, the $PEt_3$ adduct **6** was characterized by a single-crystal X-ray diffraction analysis (vide infra). In the $^{13}C$ NMR spectrum, the silaacyl carbons in **5** and **6** appear as broad singlets at room temperature (**5**-$^{13}C$: δ 80.5; **6**-$^{13}C$: δ 78.0). At −60 °C, however, **6**-$^{13}C$ displays resolvable P–C coupling ($^1J_{PC}$ = 7.5 Hz). The $^1J_{PC}$ coupling for **6**-$^{13}C$ could not be resolved in $^{13}C$ or $^{31}P$ CP-MAS NMR spectra of a solid sample.

Solutions (benzene-$d_6$ or diethyl ether) of these compounds are intensely colored (**5**, dark blue; **6**, deep purple; **7**, dark red). Compounds **5** and **6** decompose to a mixture of products (by $^1$H NMR) within a few hours at room temperature, whereas **7** decomposes cleanly with elimination of MeCl to the $\eta^4$-phosphonatosilaacyl(2−) complex $Cp^*Cl_2Ta[\eta^4$-$OC(SiMe_3)P(OMe)_2O]$.[15d] The decomposition of **5** is slightly faster than that of **6** under the same conditions. Addition of excess phosphine or CO did not significantly influence the solution stability of **5** or **6**. Although the latter decomposition products were not identified, it was apparent that neither **1** nor **2** was formed (by $^1$H and $^{13}C$ NMR).

Silaacyl **2** reacts with diphenyldiazomethane to form a different kind of adduct that does not possess a Ta–C(acyl) bond (eq 12).

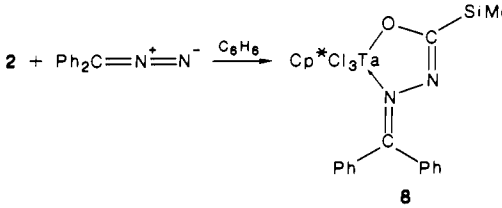


(12)

**8**

Compound **8** was isolated as bright yellow crystals from diethyl ether in 57% yield. Infrared stretches for the benzophenone silaacylhydrazonato ligand were observed at 1555 $cm^{-1}$ ($\nu_{CN}$) and 1210 $cm^{-1}$ ($\nu_{CO}$). For the labeled derivative **8**-$^{13}C$, prepared from $Ph_2CN_2$ and **2**-$^{13}C$, these absorptions shift to 1540 and 1182 $cm^{-1}$, respectively. The $SiMe_3$ resonance in the $^1$H NMR spectrum of **8**-$^{13}C$ is split into a doublet ($^3J_{CH}$ = 1.9 Hz). The $Ph_2C$ carbon is coupled to the TaO*C* carbon ($^3J_{CC}$ = 9.5 Hz) in **8**-$^{13}C$. The latter coupling constant is in the range typically observed for

three-bond couplings in aromatic systems (e.g., $^3J_{CC}$ = 8.6 Hz in iodobenzene[17]), suggesting there may be some degree of delocalization within the chelate ring of **8**.

A single-crystal X-ray diffraction study shows that bonding in the molecule is well represented by the structure shown in eq 12.[15c] The structure of this adduct is therefore fundamentally different from that of the adducts described earlier (**3–7**), since rupture of the Ta–C(acyl) bond has occurred, resulting in a complex containing a silaacylhydrazonato(1−) ligand. The silaacyl adduct **8** is inert toward exchange of $Ph_2CN_2$ with other Lewis bases (pyr or $PMe_3$, excess, benzene-$d_6$, 1 day).

In NMR tube reactions, it was apparent that a second minor (<30%) product was formed when equimolar amounts of $Ph_2CN_2$ and **2**-$^{13}C$ were combined in benzene-$d_6$. This complex could not be isolated in pure form from preparative-scale reactions. From NMR data (see Experimental Section) the product appears to contain a $^{13}C(SiMe_3)$ group in which the $^{13}C$ atom resonates in the region expected for an $sp^2$-hybridized carbon ($\delta$ 195.9).[17] The exact nature of this complex is still unknown.

Low-temperature $^{13}C$ NMR experiments in toluene-$d_8$ failed to provide evidence for the formation of adducts between the silaacyl **2** and ethers or thioethers. The $^{13}C$ NMR spectrum of **2**-$^{13}C$ at −65 °C was unaffected by the addition of 4 equiv of diethyl ether, tetrahydrofuran, 2-methyltetrahydrofuran, propylene oxide, or 2-methyltetrahydrothiophene.

**Reactions of Silaacyl Adducts $Cp^*Cl_3Ta[\eta^2\text{-}OC(L)SiMe_3]$.** Much of the reactivity of these adducts appears to be dominated by the lability of the complexed Lewis donor. For the pyridine complex **3** this lability was demonstrated by reaction with excess (ca. 10 equiv) pyridine-$d_5$, which rapidly liberates 1 equiv of pyridine (by $^1H$ NMR, eq 13). The kinetics of this exchange

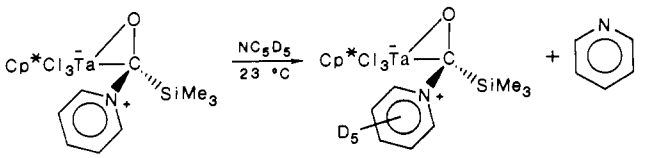


**3** **3**-$d_5$ (13)

reaction were conveniently followed at −15 °C by $^1H$ NMR under pseudo-first-order conditions with excess pyridine-$d_5$ (15–45 equiv, 99 atom % deuteriated) in toluene-$d_8$. Disappearance of the resonances due to complexed pyridine was followed and used to determine reaction rates. No intermediates were detected under these conditions (or at −70 °C with 45 equiv of pyridine-$d_5$). The exchange rate at this temperature ($k_1$ = (6.6 ± 0.8) × $10^{-4}$ $s^{-1}$) was independent of pyridine-$d_5$ concentration and is consistent with a simple dissociative ($S_N1$) mechanism (eq 14). The pyridine

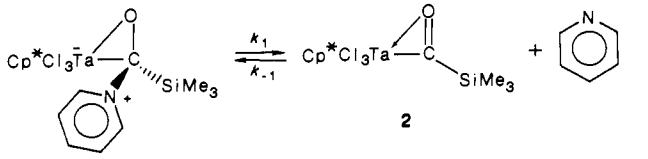


**3** **2** (14)

in **3** is readily substituted by stronger bases such as 4-methylpyridine (eq 15). The equilibrium constant for this reaction was determined by $^1H$ NMR in benzene-$d_6$ at 34 °C. Complex **9** was isolated as an orange crystalline solid from a procedure analogous to that used to obtain **3**. NMR data for **9** are presented in Table I.

Phosphines ($PMe_3$, $PEt_3$) also displace pyridine from **3**. For example, addition of $PMe_3$ (1 equiv) to a benzene-$d_6$ solution of **3** initially results in formation of a purple solution of **5** in >90% yield by $^1H$ NMR (eq 16). However, when the solution was

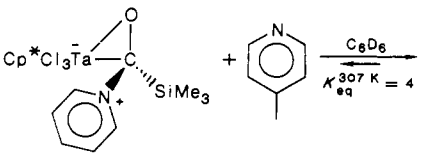


**3**

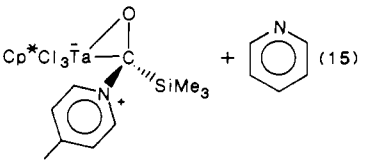


**9**

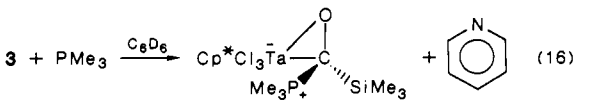


**5**

allowed to stand, the color changed to dark orange, and a new product (**10**) was detected by $^1H$ NMR. Pale yellow **10** was subsequently isolated as a stable, crystalline material from preparative-scale reactions using either **5** or **6** and pyridine (>1 equiv, eq 17). Use of **5**-$^{13}C$ in reaction 17 gives **10**-$^{13}C$, which

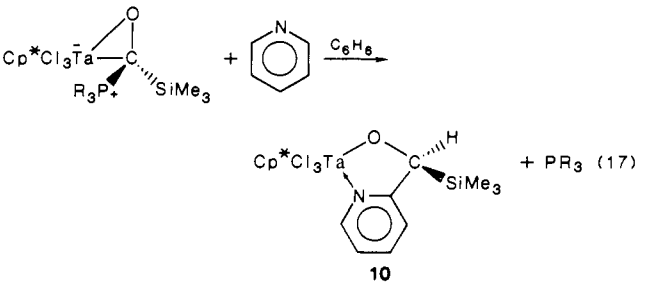


**10**

exhibits a $^{13}CO$-derived peak at $\delta$ 88.77 (d, $^1J_{CH}$ = 139 Hz) in the $^{13}C$ NMR spectrum. This peak appears as a 1:1:1 triplet ($\delta$ 88.30, $^1J_{CD}$ = 22 Hz) when pyridine-$d_5$ is employed in the preparation. In addition, the pyridine ortho carbon atom (C-2) in the five-membered heterocyclic ring appears as a doublet ($^1J_{CC}$ = 44 Hz) in **10**-$^{13}C$. The $OCHSiMe_3$ resonance appears as a singlet at $\delta$ 5.79 (1 H) for **10** and as a doublet ($^1J_{CH}$ = 139 Hz) for **10**-$^{13}C$. This signal and those due to the other aromatic protons are absent in **10**-$d_5$. $^1H$ NMR homonuclear decoupling results and exact mass spectral data also support the proposed structure.

**Reaction of 2 with $Cp_2WH_2$.** Silaacyl **2**, generated in situ, reacts with 1 equiv of $Cp_2WH_2$ to produce a dark red solution from which two new products can be isolated by fractional crystallization (eq 18). Ether-soluble **11** was isolated in 76% yield as red, moderately

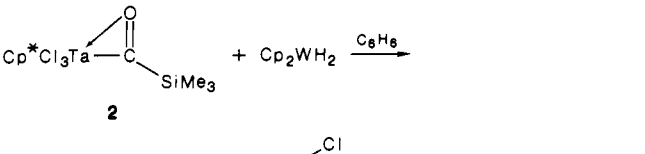


**2** **11** **12**

air-stable crystals and has been characterized by elemental analysis, exact mass spectroscopy, NMR, and its reaction with HCl (see Experimental Section). The reaction with **2**-$^{13}C$ gave **11**-$^{13}C$ with complete isotope incorporation into the methylene position ($^{13}C$ NMR: $\delta$ −26.67, $^1J_{CH}$ = 115 Hz, $J_{WC}$ = 28 Hz). As monitored by $^1H$ or $^{13}C$ NMR the reaction in eq 18 is complete within 5 min at −70 °C. No intermediates were observed at this temperature.

The tantalum-containing product **12** is sparingly soluble in toluene and is tentatively identified as $[Cp^*Cl_2TaO]_n$ based on elemental, IR, and NMR analysis. Accurate molecular weight

(17) (a) Breitmaier, E.; Voelter, W. *$^{13}C$ NMR Spectroscopy*; Verlag Chemie: Weinheim, New York, 1978. (b) Abraham, R. J.; Loftus, P. *Proton and Carbon-13 NMR Spectroscopy*; Wiley: New York, 1983. (c) Becker, E. D. *High Resolution NMR. Theory and Chemical Applications*, 2nd ed.; Academic: New York, 1980; p 102.

determinations were hampered by the low solubility of **12** in unreactive solvents. Recently, a possibly related tantalum $\mu$-oxo derivative, $[Cp^*Cl_3Ta]_2(\mu\text{-}O)$, was reported.[18]

**Reactions of 2 with Carbon Monoxide.** When pressurized with CO (10–100 psi), orange diethyl ether solutions of **2** gradually darken and deposit a brown precipitate. Filtration, concentration, and cooling of this solution allowed isolation of the alkoxy ester derivative **13** in moderate yield as a yellow-orange powder. Identical results were obtained when diethyl ether solutions of **1** were pressurized with CO under similar conditions (eq 19).

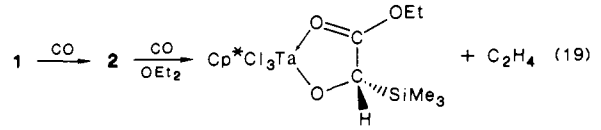


**13**

Ethylene was detected by GC/MS analysis of the volatiles from the reaction. Compound **13** has been characterized by elemental, NMR, IR, and exact mass spectroscopic analysis and by the independent preparation of a derivative (vide infra). Use of $^{13}CO$ in the carbonylation of **1** clearly identified the chelate ring carbons of **13** as those derived from carbon monoxide. The resulting complex, **13**-$^{13}C_2$, exhibits a lower $\nu_{CO}$ stretching frequency (1578 $cm^{-1}$) than **13** (1610 $cm^{-1}$) and a $^{13}C$–$^{13}C$ coupling constant ($^1J_{CC}$ = 52 Hz) consistent with directly bonded $sp^2$ and $sp^3$ carbon atoms.[17a]

With a 1:1 mixture of $(C_2H_5)_2O/(C_2D_5)_2O$ as solvent, the reaction in eq 19 produced a $C_2H_4/C_2D_4$ ratio of 1.9 (4), as determined by GC/MS analysis of the volatiles.

The ether-insoluble residues from this reaction contained a mixture of products by $^1H$ NMR (benzene-$d_6$). Although these compounds could not be characterized, it was apparent from infrared spectroscopy that terminal TaCO derivatives were present (<ca. 10%).

The reaction of **13** with $KOSiMe_3$ in tetrahydrofuran results in protiodesilylation[19] to **14** (eq 20). This conversion introduces

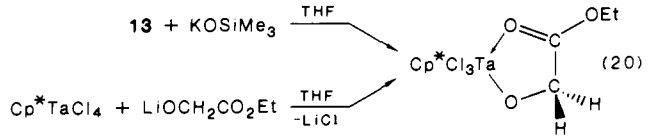


**14**

a molecular plane of symmetry that simplifies the $^1H$ NMR resonance of the diastereotopic methylene protons of **13** to a binomial quartet. It is assumed that the new proton in **14** originates from the THF solvent. Complex **14** was further characterized by an independent synthesis from $Cp^*TaCl_4$ and $LiOCH_2CO_2Et$ (eq 20).

The ether-cleavage process of eq 19 appears to depend on the availability of $\beta$-hydrogens in the ether substrate. Reaction of **1** with CO (50 psi) and 2-methyltetrahydrofuran (either as solvent or 1 equiv in pentane) leads to the ring-opened product **15** (eq 21). In contrast, with tetrahydrofuran as solvent, no evidence

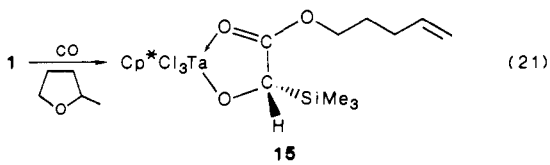


**15**

was obtained for cleavage of the ether linkage. Instead, the Ta(III) product **16** and $Me_3SiCl$ (detected by GC/MS and $^1H$ NMR) were obtained in a reaction that may be viewed as a ligand-induced reductive elimination from **1** (eq 22). The tetrahydrofuran ligand in **16** is quite labile and is readily displaced by stronger donors

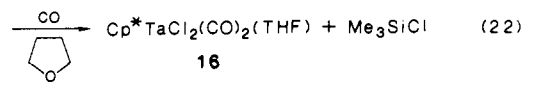


**16**

such as $PMe_3$ to afford purple $Cp^*TaCl_2(CO)_2PMe_3$ (**17**).

Attempts were also made to obtain products from carbonylation of **1** in the presence of the following ethers as solvent: propylene oxide, *n*-propyl ether, 2-methylthiophene, 2-methyltetrahydrothiophene, allyl ether, ethyl allyl ether, and phenyl allyl ether. None of these reactions provided a tractable product. $^1H$ NMR analysis of the solid materials obtained following workup indicated the formation of complex mixtures. As in the case of the reaction with diethyl ether, traces of carbonyl (TaCO) complexes were detected by infrared spectroscopy.

As described earlier, the DMP adduct **4** can be isolated by precipitation from pentane, but it dissociates extensively in benzene to regenerate **2** and free DMP. If more CO is added to such a solution, a further reaction takes place to yield the "ketene-trapped" product **18** in high yield (eq 23). Alternatively, **18** may

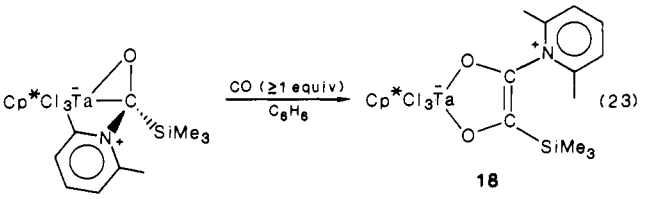


**4** **18**

be prepared by carbonylation of benzene solutions of **1** in the presence of DMP (>1 equiv); the results of both methods were identical. Dark red, air-stable crystals of **18** were isolated in 78% yield after recrystallization from cold toluene solution.

The reaction in eq 23 may be conveniently followed by $^{13}C$ NMR. Addition of $^{13}CO$ (4 equiv) to a benzene-$d_6$ solution of **1** and DMP (1 equiv) results initially in smooth conversion to silaacyl **2**. The peak due to **2** ($\delta$ 351) is then slowly replaced by two doublets ($\delta$ 139.7, 149.7; $^1J_{CC}$ = 84 Hz) assigned to the $^{13}C{=}^{13}C$ portion of **18**. At no time during this reaction were other resonances derived from $^{13}CO$ observed.

Carbonylation of pentane solutions of silyl complex **1** in the presence of $PCy_3$ (>1 equiv) results in the direct formation of ketene adduct **19** (eq 24). No evidence was found for any

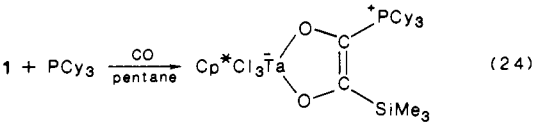


**19**

intermediates in this reaction. At −65 °C, there is no interaction between **2**-$^{13}C$ and $PCy_3$ (by $^{13}C$ NMR spectroscopy). Physical and spectroscopic properties for **19** are similar to those of the analogous DMP complex **18**. In the $^{13}C$ and $^{31}P$ NMR spectra of **19**-$^{13}C_2$ each labeled carbon atom appears as a doublet of doublets from coupling to both $^{13}C$ and $^{31}P$ nuclei. Conformation of the structure of these adducts was provided by a single-crystal X-ray analysis of **19** (vide infra).

Both **18** and **19** are unreactive toward MeI (2 equiv) in benzene-$d_6$ over 2 days at room temperature. There is no sign of decomposition when either compound is heated to 90 °C for 3 days in benzene-$d_6$. The $PCy_3$ derivative **19** is unreactive toward tetrahydrofuran or 2-methyltetrahydrofuran over a period of 2 days at 90 °C (5 equiv, benzene-$d_6$).

**Related Chemistry of the Acyl $Cp^*Cl_3Ta(\eta^2\text{-}COCH_2CMe_3)$ (21).** To evaluate the role of the silyl group in the observed reactivity of **2**, we have examined an analogous acyl complex of tantalum. The starting tantalum alkyl $Cp^*Cl_3TaCH_2CMe_3$ (**20**) was obtained straightforwardly in 54% yield from reaction of $Cp^*TaCl_4$ with $Me_3CCH_2MgCl$. Spectroscopic properties for **20** are identical with those described in the original preparation.[20] Carbonylation

(18) Jernakoff, P.; de Meric de Bellefon, C.; Geoffroy, G. L.; Rheingold, A. L.; Geib, S. J. *Organometallics* **1987**, *6*, 1362.

(19) Hudrlik, P. F.; Hudrlik, A. M.; Kulkarni, A. K. *J. Am. Chem. Soc.* **1982**, *104*, 6809.

(20) Wood, C. D.; McLain, S. J.; Schrock, R. R. *J. Am. Chem. Soc.* **1979**, *101*, 3210.

**Table I.** NMR Data for New Compounds

| compd[a] | $^1$H NMR, $\delta$ | $^{13}$C NMR, $\delta$ | $^{31}$P{$^1$H}, $\delta$ |
|---|---|---|---|
| Cp*$Cl_3$Ta($\eta^2$-COSi$Me_3$) (**2**) | 0.43 (s, 9 H, $SiMe_3$)<br>2.11 (s, 15 H, $C_5Me_5$) | | |
| Cp*$Cl_3$Ta($\eta^2$-$^{13}$COSi$Me_3$) (**2**-$^{13}$*C*)[b,c] | 0.43 (d, $^3J_{CH}$ = 1.9 Hz, 9 H, $SiMe_3$) | 351.0 (O$^{13}$*C*Si*Me*$_3$)<br>0.27 ($SiMe_3$) | |
| Cp*$Cl_3$Ta[$\eta^2$-OC(pyr)Si$Me_3$] (**3**) | 0.16 (s, 9 H, $SiMe_3$)<br>2.24 (s, 15 H, $C_5Me_5$)<br>6.29 (t, *J* = 6.9 Hz, 1 H, pyr)<br>6.41 (t, *J* = 6.3 Hz, 1 H, pyr)<br>6.53 (t, *J* = 7.8 Hz, 1 H, pyr)<br>7.63 (d, *J* = 6.0 Hz, 1 H, pyr)<br>8.41 (d, *J* = 7.5 Hz, 1 H, pyr) | 11.92 ($C_5$*Me*$_5$)<br>117.1 (O*C*(pyr))<br>124.6, 125.3, 125.8, 137.1, 141.2 (pyr)<br>127.4 (*C*$_5$Me$_5$) | |
| Cp*$Cl_3$Ta[$\eta^2$-O$^{13}$C(pyr)Si$Me_3$] (**3**-$^{13}$*C*)[b] | 0.16 (d, $^3J_{CH}$ = 1.2 Hz, 9 H, $SiMe_3$)<br>8.41 (t, *J* = 3.6 Hz, 1 H, pyr) | | |
| Cp*$Cl_3$Ta[$\eta^2$-O$^{13}$C(DMP)Si$Me_3$] (**4**-$^{13}$*C*)[d] | | 1.32 ($SiMe_3$)<br>13.33 ($C_5$*Me*$_5$)<br>26.19 (*Me*$_2C_5H_3N$)<br>117 (s, br, fwhm = 180 Hz, O$^{13}$*C*Si$Me_3$)<br>126–154 (*C*$_5$Me$_5$, $Me_2$*C*$_5$H$_3$N) | |
| Cp*$Cl_3$Ta[$\eta^2$-OC(P$Me_3$)Si$Me_3$] (**5**) | 0.27 (s, 9 H, $SiMe_3$)<br>1.33 (d, $^2J_{PH}$ = 12 Hz, 9 H, $PMe_3$)<br>2.22 (s, 15 H, $C_5Me_5$) | | 20.7 (v, br, fwhm = 150 Hz, $PMe_3$ |
| Cp*$Cl_3$Ta[$\eta^2$-O$^{13}$C(P$Me_3$)Si$Me_3$] (**5**-$^{13}$*C*)[b,c,e] | | 80.5 (br, s, fwhm = 17 Hz, O$^{13}$*C*Si$Me_3$) | 20.7 (br, fwhm = 13 Hz, $PMe_3$)<br>33.6 (br, $PEt_3$) |
| Cp*$Cl_3$Ta[$\eta^2$-OC(P$Et_3$)Si$Me_3$] (**6**) | 0.30 (s, 9 H, $SiMe_3$)<br>0.79 (m, 9 H, $PEt_3$)<br>1.92 (m, 6 H, $PEt_3$)<br>2.22 (s, 15 H, $C_5Me_5$) | | |
| Cp*$Cl_3$Ta[$\eta^2$-O$^{13}$C(P$Et_3$)Si$Me_3$] (**6**-$^{13}$*C*)[b,c] (**6**-$^{13}$*C*)[d] | | 78.0 (d, $^1J_{PC}$ = 7.5 Hz, O$^{13}$*C*Si$Me_3$)<br>3.16 ($SiMe_3$)<br>9.60, 15.58 (br, $PEt_3$)<br>13.20 ($C_5$*Me*$_5$)<br>83.32 (s, fwhm 88 Hz, O$^{13}$*C*P$Et_3$)<br>125.5 (*C*$_5$Me$_5$) | 38.5 (s, fwhm 150 Hz) |
| Cp*$Cl_3$Ta{$\eta^2$-OC[P(OMe)$_3$]Si$Me_3$} (**7**) | 0.15 (s, 9 H, $SiMe_3$)<br>2.18 (s, 15 H, $C_5Me_5$)<br>3.52 (d, $^2J_{PH}$ = 12.6 Hz, 9 H, P(OMe)$_3$) | | 60.70 (s, P(OMe)$_3$) |
| Cp*$Cl_3$Ta{$\eta^2$-O$^{13}$C[P(OMe)$_3$]Si$Me_3$} (**7**-$^{13}$*C*)[b,c] | | 103.1 (d, $^1J_{PC}$ = 158 Hz, O$^{13}$*C*Si$Me_3$) | |
| Cp*$Cl_3$Ta[OC(Si$Me_3$)NNCP$h_2$] (**8**) | 0.16 (s, 9 H, $SiMe_3$)<br>2.21 (s, 15 H, $C_5Me_5$)<br>7.00 (m, 6 H, Ph)<br>7.56 (m, 2 H, Ph)<br>7.75 (m, 2 H, Ph) | –2.41 ($SiMe_3$)<br>12.76 ($C_5$*Me*$_5$)<br>126.9, 127.1 (*o*-Ph)<br>129.4 (*C*$_5$Me$_5$)<br>129.7, 130.0 (*p*-Ph)<br>131.3, 132.0 (*m*-Ph)<br>139.8, 142.5 (*ipso*-Ph)<br>173.6 (O*C*Si$Me_3$)<br>177.4 ($Ph_2$*C*=N) | |
| Cp*$Cl_3$Ta[O$^{13}$C(Si$Me_3$)NNCP$h_2$] (**8**-$^{13}$*C*)[b] | 0.16 (d, $^3J_{CH}$ = 1.9 Hz, 9 H, $SiMe_3$) | 177.4 (d, $^3J_{CC}$ = 9.5 Hz, $Ph_2$*C*=N) | |
| Cp*$Cl_3$Ta[$\eta^2$-OC(4-Me-pyr)Si$Me_3$] (**9**) | 0.21 (s, 9 H, $SiMe_3$)<br>1.51 (s, 3 H, Me)<br>2.25 (s, 15 H, $C_5Me_5$)<br>6.22 (d, *J* = 6.3 Hz, 1 H, pyr)<br>6.28 (d, *J* = 6.3 Hz, 1 H, pyr)<br>7.62 (d, *J* = 6.3 Hz, 1 H, pyr)<br>8.35 (d, *J* = 6.3 Hz, 1 H, pyr) | 0.35 ($SiMe_3$)<br>11.97 ($C_5$*Me*$_5$)<br>20.51 (Me)<br>116.7 (O*C*Si$Me_3$)<br>125.5, 126.6, 136.6, 140.7, 151.2 (pyr)<br>126.4 (*C*$_5$Me$_5$) | |
| Cp*$Cl_3$Ta[OCH(Si$Me_3$)-*o*-$C_5H_4$N] (**10**) | 0.01 (s, 9 H, $SiMe_3$)<br>2.30 (s, 15 H, $C_5Me_5$)<br>5.79 (s, 1 H, OCH)<br>6.42 (t, *J* = 6.6 Hz, 1 H, pyr) | –1.61 (q, $J_{CH}$ = 120 Hz, $SiMe_3$)<br>12.75 (q, $J_{CH}$ = 129 Hz, ($C_5$*Me*$_5$)<br>88.77 (d, $J_{CH}$ = 139 Hz, O*C*H) | |

**Table I** (Continued)

| compd[a] | $^1$H NMR, $\delta$ | $^{13}$C NMR, $\delta$ | $^{31}$P{$^1$H}, $\delta$ |
|---|---|---|---|
| $Cp^*Cl_3\overline{Ta[OCH(SiMe_3)\text{-}o\text{-}C_5H_4N]}$ (**10**) | 6.64 (d, $J$ = 8.1 Hz, 1 H, pyr)<br>6.85 (t, $J$ = 7.7 Hz, 1 H, pyr)<br>10.09 (d, $J$ = 5.9 Hz, 1 H, pyr) | 117.4 (dd, $J_{CH}$ = 165 Hz, 7 Hz, pyr-C3)<br>121.8 (dt, $J_{CH}$ = 169 Hz, 7 Hz, pyr-C5)<br>127.6 (s, $C_5Me_5$)<br>137.3 (dd, $J_{CH}$ = 166 Hz, 9 Hz, pyr-C4)<br>150.5 (dt, $J_{CH}$ = 185 Hz, 6 Hz, pyr-C6)<br>166.6 (s, pyr-C2) | |
| $Cp^*Cl_3\overline{Ta[O^{13}CH(SiMe_3)\text{-}o\text{-}C_5H_4N]}$ (**10**-$^{13}C$)[b] | 0.01 (d, $^3J_{CH}$ = 1.6 Hz, 9 H, $SiMe_3$)<br>5.79 (d, $^1J_{CH}$ = 139 Hz, 1 H, $O^{13}CH$) | 88.78 (v strong, d, $J$ = 139 Hz, $O^{13}CH$)<br>166.6 (d, $J_{CC}$ = 44 Hz, pyr-C2) | |
| $Cp^*Cl_3\overline{Ta[O^{13}CD(SiMe_3)\text{-}o\text{-}C_5D_4N]}$ (**10**-$^{13}C$-$d_5$) | | 88.30 (t, $^1J_{CD}$ = 22 Hz, $O^{13}CD$) | |
| $Cp_2W(CH_2SiMe_3)Cl$ (**11**) | −0.14 (s, 2 H, $^2J_{WH}$ = 3.2 Hz, $CH_2$)<br>0.09 (s, 9 H, $SiMe_3$)<br>4.45 (s, 10 H, $C_5H_5$) | −26.67 (t, $J_{CH}$ = 115 Hz, $J_{WC}$ = 28 Hz, $CH_2$)<br>3.60 (q, $J_{CH}$ = 118 Hz, $SiMe_3$)<br>90.36 (dq, $J_{CH}$ = 181 Hz, 6 Hz, $C_5H_5$) | |
| $Cp_2W(^{13}CH_2SiMe_3)Cl$ (**11**-$^{13}C$)[b] | −0.14 (d, $^1J_{CH}$ = 115 Hz, $^{13}CH_2$)<br>0.09 (d, $^3J_{CH}$ = 1.4 Hz, 9 H, $SiMe_3$) | −26.68 (v strong, t, $J_{CH}$ = 115 Hz, $^{13}CH_2$) | |
| $[Cp^*Cl_2TaO]_n$ (**12**) | 2.21 ($C_5Me_5$) | 12.78 (q, $^1J_{CH}$ = 129 Hz, $C_5Me_5$) ($C_5Me_5$ resonance obscured by solvent) | |
| $Cp^*Cl_3\overline{Ta[OCH(SiMe_3)C(O)OEt]}$ (**13**)[f] | 0.08 (s, 9 H, $SiMe_3$)<br>0.75 (t, $J$ = 7 Hz, 3 H, $OCH_2CH_3$)<br>2.29 (s, 15 H, $C_5Me_5$)<br>3.89 (m, 15 H, $OCH_2CH_3$)<br>5.16 (s, 1 H, OCH) | −1.90 (q, $J_{CH}$ = 120 Hz, $SiMe_3$)<br>12.90 (q, $J_{CH}$ = 126 Hz, $C_5Me_5$)<br>13.90 (q, $J_{CH}$ = 128 Hz, $OCH_2CH_3$)<br>66.9 (t, $J_{CH}$ = 154 Hz, $OCH_2CH_3$)<br>84.8 (d, $J_{CH}$ = 137 Hz, $OCHSiMe_3$)<br>128.2 ($C_5Me_5$)<br>189.8 (s, COOEt) | |
| $Cp^*Cl_3\overline{Ta[O^{13}CH(SiMe_3)^{13}C(O)OEt]}$ (**13**-$^{13}C_2$)[b,f] | 0.08 (d, $^3J_{CH}$ = 1.9 Hz, 9 H, $SiMe_3$)<br>5.16 (dd, $^1J_{CC}$ = 137 Hz, $^2J_{CH}$ = 6 Hz, 1 H, $O^{13}CH$) | 84.8 (d, $^1J_{CC}$ = 52 Hz, $O^{13}CH$)<br>189.8 (d, $^1J_{CC}$ = 52 Hz, $^{13}COOEt$) | |
| $Cp^*Cl_3\overline{Ta[OCH_2C(O)OEt]}$ (**14**)[f] | 0.66 (t, $J$ = 7 Hz, 3 H, $OCH_2CH_3$)<br>2.20 (s, 15 H, $C_5Me_5$)<br>3.79 (q, $J$ = 7 Hz, $OCH_2$) | 12.9 ($C_5Me_5$)<br>14.2 ($OCH_2CH_3$)<br>67.9 ($OCH_2CH_3$)<br>76.2 ($OCH_2COOEt$)<br>129.6 ($C_5Me_5$)<br>187.3 (COOEt) | |
| $Cp^*Cl_3\overline{Ta[OCH(SiMe_3)C(O)O(CH_2)_3CH{=}CH_2]}$ (**15**)[f] | 0.10 (s, 9 H, $SiMe_3$)<br>1.32 (m, 2 H, $OCH_2CH_2$)<br>1.68 (q, 2 H, $J$ = 7 Hz, $CH_2CHCH_2$)<br>2.29 (s, 15 H, $C_5Me_5$)<br>3.98 (m, 2 H, $OCH_2$)<br>4.87 (m, 2 H, $CHCH_2$)<br>5.17 (s, 1 H, OCH)<br>5.45 (m, 1 H, $CHCH_2$) | −1.90 ($SiMe_3$)<br>12.9 ($C_5Me_5$)<br>27.7, 29.7 ($CH_2CH_2CHCH_2$)<br>70.1 ($OCH_2$)<br>84.8 ($OCHSiMe_3$)<br>115.7 ($CHCH_2$)<br>128.3 ($C_5Me_5$)<br>136.9 ($CHCH_2$)<br>189.8 ($CO_2CH_2$) | |
| $Cp^*Cl_2Ta(CO)_2(THF)$ (**16**) | 1.28 (m, 4 H, THF)<br>1.73 (s, br, 15 H, $C_5Me_5$)<br>3.79 (m, 4 H, THF) | | |
| $Cp^*Cl_2Ta(CO)_2(PMe_3)$ (**17**) | 1.25 (d, $^2J_{PC}$ = 12 Hz, 9 H, $PMe_3$)<br>1.74 (s, 15 H, $C_5Me_5$) | 12.96 ($C_5Me_5$)<br>16.61 (d, $^1J_{PC}$ = 27 Hz, $PMe_3$)<br>105.1 ($C_5Me_5$)<br>236.3 (d, $^2J_{PC}$ = 11 Hz, CO) | −31.9 ($PMe_3$) |
| $Cp^*Cl_3\overline{Ta[OC(SiMe_3)C(DMP)O]}$ (**18**) | −0.29 (s, 9 H, $SiMe_3$)<br>2.44 (s, 15 H, $C_5Me_5$)<br>2.69 (s, 6 H, $Me_2C_5H_3N$) | −2.51 ($SiMe_3$)<br>13.05 ($C_5Me_5$)<br>21.97 ($Me_2C_5H_3N$) | |

Table I (Continued)

| compd[a] | $^1$H NMR, δ | $^{13}$C NMR, δ | $^{31}$P{$^1$H}, δ |
|---|---|---|---|
| $Cp^*Cl_3Ta[OC(SiMe_3)C(DMP)O]$ (**18**) | 7.09 (d, $J$ = 8 Hz, 1 H, DMP)<br>8.26 (t, $J$ = 8 Hz, 2 H, DMP) | 126.3 ($C_5Me_5$)<br>139.7 ($OC$(DMP))<br>149.7 ($OC$(SiMe$_3$)) | |
| $Cp^*Cl_3Ta[O^{13}C(SiMe_3)^{13}C(DMP)O]$ (**18**-$^{13}C_2$)[b] | −0.29 (d, $^3J_{CH}$ = 1.5 Hz, SiMe$_3$) | 139.7 (d, $J_{CC}$ = 84 Hz, O$^{13}C$(DMP))<br>149.7 (d, $J_{CC}$ = 84 Hz, O$^{13}C$(SiMe$_3$)) | |
| $Cp^*Cl_3Ta[OC(SiMe_3)C(PCy_3)O]$ (**19**) | 0.34 (s, 9 H, SiMe$_3$)<br>1.1, 1.6, 1.9 (br, 33 H, PCy$_3$)<br>2.45 (s, 15 H, $C_5Me_5$) | 1.40 (SiMe$_3$)<br>13.30 ($C_5Me_5$)<br>25.8, 26.9, 27.4 (PCy$_3$)<br>32.1 (d, $^1J_{PC}$ = 43 Hz, PCy$_3$)<br>125.9 ($C_5$Me$_5$)<br>136.3 (d, $^1J_{PC}$ = 100 Hz, $OC$(PCy$_3$))<br>161.0 (d, $^2J_{PC}$ = 42 Hz, $OC$(SiMe$_3$)) | 27.4 (PCy$_3$) |
| $Cp^*Cl_3Ta[O^{13}C(SiMe_3)^{13}C(PCy_3)O]$ (**19**-$^{13}C_2$)[b] | 0.34 (d, $^3J_{CH}$ = 1.6 Hz, SiMe$_3$) | 136.3 (dd, $^1J_{PC}$ = 100 Hz, $J_{CC}$ = 68 Hz, O$^{13}C$(PCy$_3$))<br>161.0 (dd, $^2J_{PC}$ = 42 Hz, $J_{CC}$ = 68 Hz, O$^{13}C$(SiMe$_3$)) | 27.4 (dd, $^1J_{PC}$ = 100 Hz, $^2J_{PC}$ = 42 Hz) |
| $Cp^*Cl_3Ta(\eta^2$-$COCH_2CMe_3)$ (**21**) | 1.21 (s, 9 H, CMe$_3$)<br>2.12 (s, 15 H, $C_5Me_5$)<br>3.20 (s, 2 H, CH$_2$) | 11.77 ($C_5Me_5$)<br>30.13 ($CMe_3$)<br>54.87 (CH$_2$)<br>130.7 ($C_5$Me$_5$)<br>316.0 ($COCH_2$) | |
| $Cp^*Cl_3Ta(\eta^2$-$^{13}COCH_2CMe_3)$ (**21**-$^{13}C$)[b,c] | 1.27 (s, 9 H, CMe$_3$)<br>2.10 (s, 15 H, $C_5Me_5$)<br>2.99 (d, $^2J_{CH}$ = 6 Hz, 2 H, CH$_2$) | 316.0 (s, $^{13}COCH_2$) | |
| $Cp^*Cl_3Ta(\eta^2$-$^{13}COCH_2CMe_3)$(pyr) (**22**-$^{13}C$)[c] | 0.63 (s, 9 H, CMe$_3$)<br>2.06 (s, 15 H, $C_5Me_5$)<br>2.78 (dd, $^2J_{HH}$ = 21<br>3.45 (dd, $^2J_{HH}$ = 21 Hz, $^2J_{CH}$ = 5 Hz, 1 H, CH$_2$)<br>6.27 (m, 2 H, pyr)<br>6.60 (m, 1 H, pyr)<br>9.26 (d, $J$ = 5 Hz, 2 H, pyr) | 313.3 (s, $^{13}COCH_2$) | |
| $Cp^*Cl_3Ta(cis$-OCH=CHCMe$_3)$(pyr) (**23**) | 1.19 (s, 9 H, CMe$_3$)<br>2.34 (s, 15 H, $C_5Me_5$)<br>3.90 (d, $J$ = 7 Hz, 1 H, OCH$CH$)<br>6.18 (d, $J$ = 7 Hz, 1 H, OCH)<br>6.55 (t, $J$ = 7 Hz, 2 H, pyr)<br>6.75 (t, $J$ = 7 Hz, 1 H, pyr)<br>9.59 (s, br, 2 H, pyr) | 12.96 ($C_5Me_5$)<br>31.27 ($CMe_3$)<br>117.8 (OCHCH)<br>122.6, 137.3, 153.4 (pyr)<br>129.7 ($C_5$Me$_5$)<br>147.7 (OCH) | |
| $Cp^*Cl_3Ta(cis$-O$^{13}$CH=CHCMe$_3)$(pyr) (**23**-$^{13}C$)[b,c] | 1.20 (s, 9 H, CMe$_3$)<br>2.35 (s, 15 H, $C_5Me_5$)<br>3.88 (t, $J$ = 7 Hz, 1 H, O$^{13}$CHC$H$)<br>6.11 (dd, $^2J_{HH}$ = 7 Hz, $^1J_{CH}$ = 183 Hz, 1 H, O$^{13}$C$H$)<br>6.61 (t, $J$ = 7 Hz, 2 H, pyr)<br>6.84 (t, $J$ = 7 Hz, 1 H, pyr)<br>9.50 (s, br, 2 H, pyr) | 147.7 (d, $^1J_{CH}$ = 183 Hz, O$^{13}CH$) | |

[a] Spectra recorded in benzene-$d_6$ at 22 °C on the GE QE 300 unless stated otherwise. [b] Remainder of spectrum identical with that of unlabeled compound. [c] Toluene-$d_8$, −65 °C. [d] Solid-state CP-MAS spectrum. [e] 50 MHz ($^{13}$C), or 81 MHz ($^{31}$P). [f] 360 MHz ($^1$H) or 50 MHz ($^{13}$C), 22 °C.

of **20** proceeds smoothly in pentane or benzene as shown in eq 25. Complex **21**-$^{13}C$, obtained from **20** and $^{13}$CO, exhibits a sharp

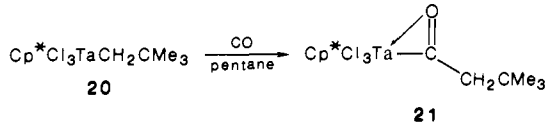


20 21 (25)

singlet at δ 316.2 in its $^{13}$C NMR spectrum. Compared to the analogous silaacyl complex **2**, the $^{13}$C resonance of the acyl carbon in **21** exhibits an upfield shift of 34 ppm. In common with silaacyl **2**, the acyl resonance in **21** is rather broad at room temperature (fwhm = 15 Hz).

Whereas **2** decomposes rapidly at room temperature, **21** is stable for an indefinite period both as a solid and in hydrocarbon or ethereal solvents. In addition, **21** is inert toward further reaction with CO and is recovered unchanged after 3 days in benzene under 100 psi of CO.

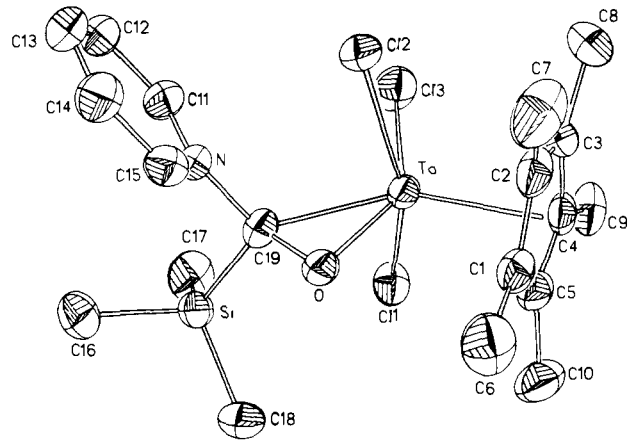


**Figure 2.** Molecular structure and labeling scheme for $Cp^*Cl_3Ta[\eta^2\text{-}OC(pyr)SiMe_3]$ (**3**).

Addition of pyridine (1 equiv) to a toluene-$d_8$ solution of **21** at −65 °C results in rapid reaction to produce the *metal-bound* pyridine adduct **22**, characterized spectroscopically (eq 26).

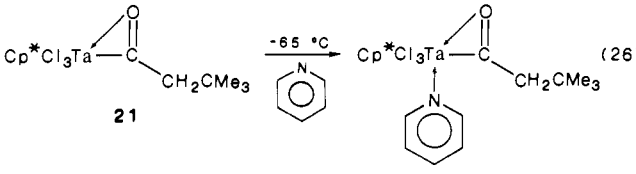


**21** **22** (26)

Conversion of **21** to **22** results in a relatively small upfield shift of the acyl carbon from δ 316.2 to δ 313.3. As expected, the ortho hydrogens of the pyridine ligand in **22** resonate at low field relative to free pyridine[17b] and are equivalent by $^1H$ NMR down to −70 °C (see Table I). The methylene protons of **22**-$^{13}C$ are inequivalent, and each appears as a doublet of doublets due to geminal and $^{13}C$ coupling ($^2J_{HH}$ = 21 Hz; $^2J_{CH}$ = 5 Hz).

Complex **22**-$^{13}C$ is stable for hours below −40 °C, but as the temperature is raised to ca. −10 °C the peak at δ 313.3 is slowly replaced by a new peak at δ 147.7, which appears as a doublet ($^1J_{CH}$ = 183 Hz) in the gated spectrum. This latter resonance is assigned to the new complex **23**, which has been isolated in high yield from preparative-scale reactions (eq 27). Spectroscopic data

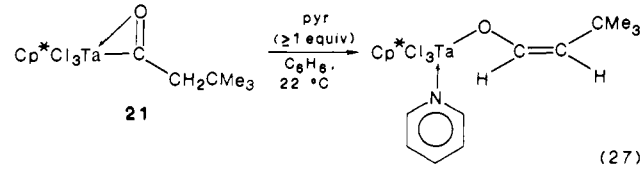


**21** **23** (27)

for **23** are presented in Table I. Parameters associated with the *cis*-enolate ligand are similar to those found in the analogous complex $Cp^*_2Th(OCHCHCMe_3)Cl$.[21] Compound **23** is stable indefinitely at −45 °C in the solid state, however, it decomposes to a mixture of uncharacterized products within a few days at 22 °C under nitrogen.

**Description of the Structure of 3.** Crystals of **3** suitable for X-ray diffraction were obtained by slow cooling of a saturated toluene solution. An ORTEP view is presented in Figure 2; relevant geometrical parameters are summarized in Table II.

The tantalum coordination geometry may be described as a distorted octahedron if the $\eta^5\text{-}C_5Me_5$ ligand is considered to occupy a single coordination site and the $\eta^2\text{-}OC(SiMe_3)(NC_5H_5)$ ligand is considered to be bidentate. Distances and angles in the molecule indicate that complete reduction of the carbonyl group has occurred. Thus, the distances and angles about C(19) are typical for saturated carbon.[22] The Ta–C(19) distance of 2.214 (5) Å is comparable to Ta–C single-bond distances found in similar compounds, e.g., $Cp^*Ta(CHPh)(CH_2Ph)_2$ (av 2.21 Å),[23a] $Cp^*Cl_2Ta(C_4H_8)$ (2.22 Å),[23b] and $Cp^*Cl_2Ta(C_7H_{12})$ (av 2.20 Å).[23b]

Complexation of pyridine to the carbonyl carbon results in reduction of the C–O bond order, as seen from comparison of the C(19)–O distance (1.416 (6) Å) with the C–O distance in the silaacyl $Cp_2Zr(\eta^2\text{-}COSiMe_3)Cl$ (1.244 (3) Å).[15a] Although the $\eta^2\text{-}OC(SiMe_3)(NC_5H_5)$ ligand resembles an $\eta^2$-ketone, spectroscopic data and bond lengths and angles indicate that it derives no significant contribution from a coordinated O=C resonance hybrid[6b] (cf. C–O distances in $Cp_2V(\eta^2\text{-}CH_2O)$ (1.35 Å[24a]) and $Cp_2Mo(\eta^2\text{-}CH_2O)$ (1.36 Å[24b])). The structural characterization of organic compounds containing long intramolecular N(amine)···C(carbonyl) interactions[25] has allowed construction of a reaction coordinate for nucleophilic addition to a carbonyl group.[25a,b] In the formation of **3**, amine addition to **2** is complete,

**Table II.** Selected Bond Distances (Å) and Angles (deg) for **3**[a]

| atom 1 | atom 2 | dist | atom 1 | atom 2 | dist |
|---|---|---|---|---|---|
| Ta | CNT | 2.171 (5) | Ta | C(19) | 2.214 (5) |
| Ta | Cl(1) | 2.439 (2) | Si | C(19) | 1.925 (6) |
| Ta | Cl(2) | 2.447 (1) | O | C(19) | 1.416 (6) |
| Ta | Cl(3) | 2.469 (2) | N | C(19) | 1.493 (6) |
| Ta | O | 1.945 (3) | | | |

| atom 1 | atom 2 | atom 3 | angle |
|---|---|---|---|
| CNT | Ta | Cl(1) | 102.3 (2) |
| CNT | Ta | Cl(2) | 101.8 (2) |
| CNT | Ta | Cl(3) | 113.0 (2) |
| CNT | Ta | O | 107.5 (2) |
| CNT | Ta | C(19) | 146.5 (2) |
| O | Ta | C(19) | 39.1 (2) |
| Ta | O | C(19) | 80.7 (3) |
| Ta | C(19) | O | 60.1 (2) |
| Ta | C(19) | N | 117.2 (4) |
| O | C(19) | N | 110.7 (4) |
| O | C(19) | Si | 114.5 (3) |
| N | C(19) | Si | 109.1 (3) |

[a] CNT is the centroid of the $\eta^5\text{-}C_5Me_5$ ring.

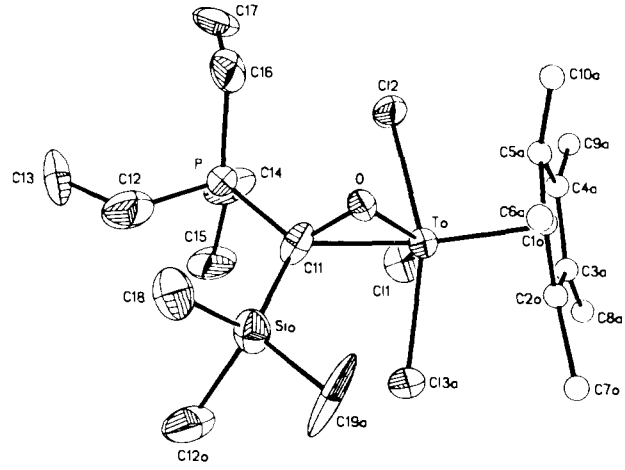


**Figure 3.** Molecular structure and labeling scheme for $Cp^*Cl_3Ta[\eta^2\text{-}OC(PEt_3)SiMe_3]$ (**6**). One half of a mirror-plane disordered structure is shown (see Experimental Section).

(21) Manriquez, J. M.; Fagan, P. J.; Marks, T. J.; Day, C. S.; Day, V. W. *J. Am. Chem. Soc.* **1978**, *100*, 7112.

(22) The C–O bond lengths in dimethyl ether and ethanol are 1.41 Å. The C–N bond in methylamine is 1.47 Å. See: March, J. *Advanced Organic Chemistry*, 3rd ed.; Wiley: New York, 1985; p 19.

(23) (a) Messerle, L. W.; Jennische, P.; Schrock, R. R.; Stucky, G. *J. Am. Chem. Soc.* **1980**, *102*, 6744. (b) Churchill, M. R.; Youngs, W. J. *Ibid.* **1979**, *101*, 6462.

(24) (a) Gambarotta, S.; Floriani, C.; Chiesi-Villa, A.; Guastini, C. *J. Am. Chem. Soc.* **1982**, *104*, 2019. (b) Gambarotta, S.; Floriani, C.; Chiesi-Villa, A.; Guastini, C. *Ibid.* **1985**, *107*, 2985.

**Table III.** Selected Bond Distances (Å) and Angles (deg) for **6**[a]

| atom 1 | atom 2 | dist | atom 1 | atom 2 | dist |
|---|---|---|---|---|---|
| Ta | CNT | 2.202 | Ta | C(11) | 2.24 (2) |
| Ta | Cl(1) | 2.442 (5) | Si(a) | C(11) | 1.95 (3) |
| Ta | Cl(2) | 2.531 (7) | O | C(11) | 1.43 (3) |
| Ta | Cl(3) | 2.389 (7) | P | C(11) | 1.81 (3) |
| Ta | O | 1.945 (16) | | | |

| atom 1 | atom 2 | atom 3 | angle |
|---|---|---|---|
| CNT | Ta | Cl(1) | 109.5 (5) |
| CNT | Ta | Cl(2) | 99.4 (5) |
| CNT | Ta | Cl(3a) | 104.0 (5) |
| CNT | Ta | O | 107.7 (7) |
| CNT | Ta | C(11) | 138.6 (9) |
| O | Ta | C(11) | 39.0 (9) |
| Ta | O | C(11) | 81.8 (13) |
| Ta | C(11) | O | 59.1 (11) |
| Ta | C(11) | P | 121.8 (14) |
| O | C(11) | P | 118.1 (22) |
| O | C(11) | Si | 104.7 (18) |
| P | C(11) | Si | 114.4 (14) |

[a] CNT is the centroid of the $\eta^5$-$C_5Me_5$ ring.

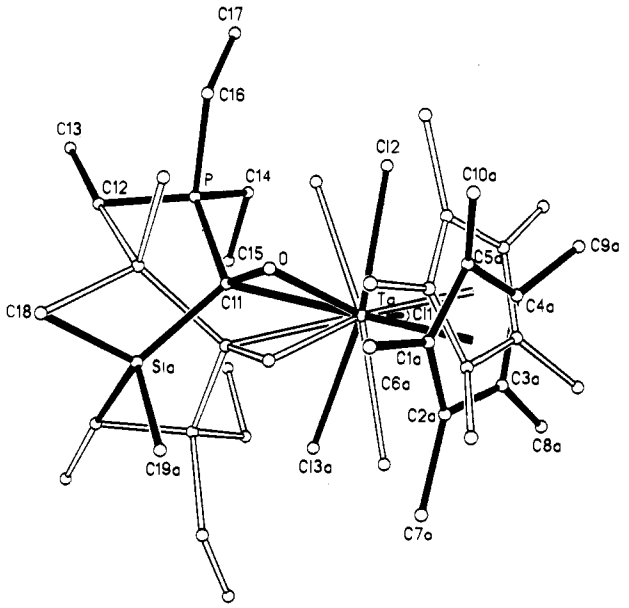


**Figure 4.** Fully disordered structure of $Cp^*Cl_3Ta[\eta^2$-$OC(PEt_3)SiMe_3]$ (**6**) showing the intertwining of mirror-plane disordered halves as the solid and open-line structures.

as evidenced by the N–C(19) distance, 1.493 (6) Å, which is in the region expected for an $N^+$–C single bond.[25c,26]

**Description of the Structure of 6.** A detailed discussion of the structure of **6** will not be attempted since the X-ray data are of relatively low precision due to structural disorder. An ORTEP view of the molecule is shown in Figure 3; Table III lists relevant distances and angles. The asymmetric unit consists of two half-occupancy molecules intertwined about a mirror plane, with Ta, Cl(1), and C(18) residing on the mirror plane (Figure 4; see Experimental Section).

Despite the disorder, the overall structure of **6** is clearly analogous to that of **3**, with the Lewis base ($PEt_3$) bonded to the carbon of the $\eta^2$-silaacyl moiety. In particular, parameters associated with the TaOC triangles are nearly identical for **3**, **6**, and $Cp^*Cl_2Ta[\eta^4$-$OC(SiMe_3)P(OMe)_2O]$.[15d] The angles within these triangles are also similar to those reported recently for the

(25) (a) Bürgi, H. B.; Dunitz, J. D.; Shefter, E. *J. Am. Chem. Soc.* **1973**, *95*, 5065. (b) Dunitz, J. D. *X-ray Analysis and the Structure of Organic Molecules*; Cornell University Press: Ithaca, NY, 1979; p 366. (c) Birnbaum, G. I. *J. Am. Chem. Soc.* **1974**, *96*, 6165.

(26) (a) Raston, C. L.; Rowbottom, G. L.; White, A. H. *J. Chem. Soc., Dalton Trans.* **1981**, 1389. (b) Tominaga, Y.; Kobayashi, G.; Tamura, C.; Sato, S.; Hata, T. *Acta Crystallogr., Sect. B* **1979**, *35*, 2443.

**Table IV.** Selected Bond Distances (Å) and Angles (deg) for **19**[a]

| atom 1 | atom 2 | dist | atom 1 | atom 2 | dist |
|---|---|---|---|---|---|
| Ta | CNT | 2.203 | O(1) | C(14) | 1.40 (2) |
| Ta | Cl(1) | 2.424 (5) | C(14) | C(15) | 1.35 (2) |
| Ta | Cl(2) | 2.437 (4) | O(2) | C(15) | 1.32 (2) |
| Ta | Cl(3) | 2.435 (4) | Si | C(14) | 1.86 (2) |
| Ta | O(1) | 1.969 (11) | C(15) | P | 1.84 (2) |
| Ta | O(2) | 2.049 (9) | | | |

| atom 1 | atom 2 | atom 3 | angle |
|---|---|---|---|
| CNT | Ta | Cl(1) | 104.2 |
| CNT | Ta | Cl(2) | 102.1 |
| CNT | Ta | Cl(3) | 102.1 |
| CNT | Ta | O(1) | 100.9 |
| CNT | Ta | O(2) | 176.8 |
| O(1) | Ta | O(2) | 79.5 (4) |
| Ta | O(1) | C(14) | 120.6 (9) |
| O(1) | C(14) | C(15) | 108 (1) |
| C(14) | C(15) | O(2) | 121 (2) |
| C(15) | O(2) | Ta | 113.8 (9) |
| C(14) | C(15) | P | 131.1 (1) |
| P | C(15) | O(2) | 108 (1) |

[a] CNT is the centroid of the $\eta^5$-$C_5Me_5$ ring.

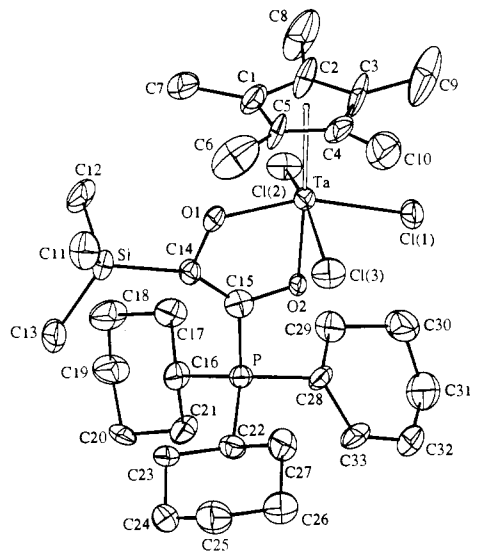


**Figure 5.** Molecular structure and labeling scheme for $Cp^*Cl_3Ta[OC(SiMe_3)C(PCy_3)O]$ (**19**).

acyl adduct $Cp(NO)(I)Mo[\eta^2$-$OC(PMe_3)(p$-$C_6H_4Me)]$.[11] However, the C–O distance in the latter compound (1.367 (6) Å) is considerably shorter than the analogous distances in **3** (1.416 (6) Å), **6** (1.43 (3) Å), and $Cp^*Cl_2Ta[\eta^4$-$OC(SiMe_3)P(OMe)_2O]$ (1.45 (2) Å).

**Description of the Structure of 19.** Dark red, monoclinic crystals of **19** were grown from concentrated toluene solution. The structure of **19** consists of discrete molecules as shown in the ORTEP view in Figure 5. Table IV contains relevant geometrical parameters. The $Cp^*TaCl_3$ portion of the molecule is similar to that in **3** and **6** and is otherwise unremarkable. The L–Ta–L angles in the O(1)–Cl(1)–Cl(2)–Cl(3) equatorial plane are approximately equal, except for the O(1)–Ta–Cl(3) angle (92.0 (3)°), which is roughly 6° larger than the other three. This is presumably due to nonbonded interactions between Cl(3) and the bulky $PCy_3$ group.

Parameters associated with the chelate ring (Ta–O(1)–C(14)–C(15)–O(2)) are similar to those in the related complex $Cp^*_2Th[OC(CH_2CMe_3)C(PMe_3)O]Cl$.[3a] The relatively short C(14)–C(15) distance, 1.35 (2) Å, suggests an important contribution from resonance structure A, although others may be considered (B, C). The P–C(15) bond length (1.84 (2) Å) is roughly equal to the remaining P–C distances (av 1.83 (2) Å). Least-squares planes were calculated for atoms O(1), Cl(1), Cl(2), Cl(3), and Ta (plane 1) and for Ta, O(1), C(14), C(15), and O(2)

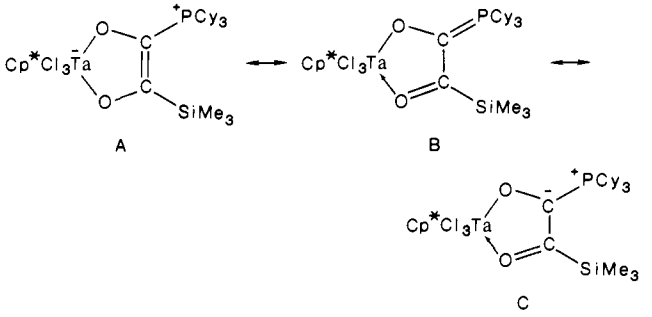


(plane 2). The dihedral angle between the two planes is 92.4°. The Ta–O(1)–C(14)–C(15)–O(2) ring is quite planar, the maximum displacement of any atom in the chelate ring from plane 2 being 0.05 (1) Å (for O(1)).

## Discussion

Carbon monoxide inserts cleanly into the tantalum–silicon bond of **1** to form the reactive $\eta^2$-silaacyl complex $Cp^*Cl_3Ta(\eta^2\text{-}CO\text{-}SiMe_3)$ (**2**). Although stable at low temperature, **2** decomposes rapidly at 20 °C in hydrocarbon solvents to give mixtures of tantalum carbonyl species and $Me_3SiCl$ by an unknown mechanism. In tetrahydrofuran, this carbonylation reaction yields a tractable Ta(III) carbonyl product, $Cp^*Cl_2Ta(CO)_2(THF)$ (**16**), along with $Me_3SiCl$ (eq 22). In a related reaction, $Cp_2Ti(SiMe_3)Cl$ eliminates $Me_3SiCl$ on carbonylation to form $Cp_2Ti(CO)_2$.[15a] These results suggest that reductive elimination of $Me_3SiCl$ and CO insertion are competing pathways in these metal–silyl systems. Complex **1** is also known to undergo ligand-induced reductive elimination reactions with a variety of other donor molecules such as phosphines, acetylenes, and organic carbonyl compounds.[16]

Although $\eta^2$-acyl complexes are known to be susceptible to nucleophilic attack at the acyl carbon,[1-5] there are few reported examples of their reactivity toward simple Lewis donors.[8-11] The $\eta^2$-silaacyl–Lewis base adducts $Cp^*Cl_3Ta[\eta^2\text{-}OC(L)SiMe_3]$ (L = pyr, DMP, $PMe_3$, $PEt_3$, $P(OMe)_3$, and 4-Me-pyr; **3–7**, **9**) are readily prepared by addition of the appropriate base to pentane solutions of **2**. Coordination of the Lewis base to the silaacyl is reversible, and the equilibrium in eq 28 is established in solution.

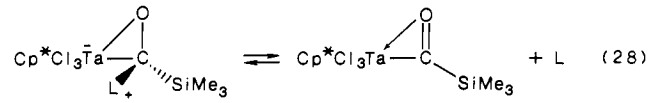


This equilibrium lies heavily to the left in the pyridine and 4-methylpyridine derivatives (**3** and **9**, respectively). In toluene-$d_8$ solution no spectroscopic evidence was found for the presence of **2** in solutions of **3** or **9** by either $^1H$ or $^{13}C$ NMR between −70 and +90 °C. The results of kinetic experiments involving exchange of the pyridine in **3** with pyridine-$d_5$, however, clearly establish that a dissociative mechanism is operative. For the DMP adduct **4**, the equilibrium in eq 28 is shifted heavily to the right in solution, and as shown by $^1H$ and $^{13}C$ NMR, **4** is completely dissociated at 22 °C in toluene-$d_8$.

On the basis of qualitative estimates using $^1H$ NMR, the tendency of Lewis bases to form adducts with **2** follows the order

$$\underset{\text{increasing tendency toward adduct formation}}{\xleftarrow{\qquad\qquad}} \quad PMe_3 > PEt_3 > \text{4-Me-pyr} > \text{pyr} \gg \text{DMP, CO (?)} > PCy_3\text{, ethers}$$

The inclusion of CO in this series is somewhat speculative since in this case "adduct" formation was not directly observed. It is obvious from comparison of the relative ordering of the three pyridine derivatives (**3**, **4**, and **9**) that both steric and electronic factors play an important role in determining stability of the adduct.

It is interesting that in the formation of the $\eta^2$-silaacyl–Lewis base adducts, the silaacyl carbon in **2** acts as the more electrophilic site, rather than the formally 16-electron tantalum center. Note that the related $\eta^2$-acyl $Cp^*Cl_3Ta(\eta^2\text{-}COCH_2CMe_3)$ (**21**) does not form observable, analogous adducts. Rather, pyridine preferentially attacks the metal center of **21** to give adduct **22**. Also, the reaction in eq 17 suggests that sterically, attack of pyridine at the tantalum center of **2** may be feasible (vide infra). Presently, an explanation for the greater electrophilic character of the CO-$SiMe_3$ ligand (compared to $COCH_2CMe_3$) is not readily apparent. Clearly, the long Si–C(silaacyl) bond should make the silaacyl carbon of **2** more susceptible to nucleophilic attack than the acyl carbon of **21**. In addition, there may be electronic factors that influence the electrophilic properties of **2**. Hoffmann and coworkers have suggested that the electrophilic character of some $\eta^2$-acyls is derived from stabilization of the $\pi^*_{CO}$ level by interaction with an unoccupied metal d orbital.[1b] In the case of **2**, additional stabilization of this energy level may result from overlap with an acceptor orbital on silicon.

Formation of the silaacyl adducts is characterized by large upfield shifts (ca. 250 ppm) in the $^{13}C$ NMR resonance of the silaacyl carbon (see Table I). These resonances occur at $\delta$ 117 in the pyridine derivatives **3**, **4**, and **9**, at ca. $\delta$ 80 in the phosphine adducts **5** and **6**, and at $\delta$ 103.1 in the $P(OMe)_3$ adduct **7** and are in the range expected for $sp^3$ carbons bearing $SiMe_3$ and oxygen substituents.[17] The phosphine adducts **5**-$^{13}C$ and **6**-$^{13}C$ both exhibit broad $O^{13}CSiMe_3$ peaks at room temperature in the $^{13}C$ NMR spectrum, perhaps due to quadrupolar broadening by the $^{181}Ta$ nucleus. Both resonances sharpen at −65 °C, but only the $PEt_3$ derivative **6**-$^{13}C$ shows resolvable $^{31}P$ coupling ($^1J_{PC}$ = 7.5 Hz). The phosphite complex **7**-$^{13}C$, on the other hand, exhibits a large phosphorus–carbon single-bond coupling constant, 158 Hz. In other M–C–P-bonded complexes, $^1J_{PC}$ values span a wide range. Examples include $[(PMe_3)_2Cl_2W{\equiv}C{-}PMe_3]_2$[27] and $\{[HB(N_2C_3Me_2H)_3](OC)_2W{\equiv}CPMe_3\}[PF_6]$,[28] which exhibit singlets for the WCP carbon in their $^{13}C$ NMR spectra, and Cp(NO)(I)Mo[$\eta^2$-OC($PMe_3$)(*p*-$C_6H_4Me$)] ($\delta$ 72.2, $^1J_{PC}$ = 60.3 Hz),[11] $Cp(CO)Fe[CMeOAlEt_2N^tBuPPh_2]$ ($\delta$ 58.4, $^1J_{PC}$ = 68.6 Hz),[8] and $(\eta^5\text{-}C_5Me_4Et)_2Cl_4Ta_2(H)(\mu\text{-}O)(\mu\text{-}CHPMe_3)$ ($\delta$ 94.3, $^1J_{PC}$ = 44 Hz).[29] In the oxoxanthate complexes $MO(S_2COR)(S_2C(PMe_3)OR)$ (M = Mo, W; R = Me, Et, $^i$Pr), which contain the zwitterionic ligands $S_2C^-(^+PMe_3)OR$, the ylide carbons appear as doublets in the $^{13}C$ NMR spectra, with $^1J_{PC}$ varying from 84 to 89 Hz.[30]

Phosphines ($PMe_3$, $PEt_3$) bind more strongly than pyridine to the silaacyl **2**. Thus, addition of $PMe_3$ to a benzene-$d_6$ solution of **3** proceeds rapidly to **5** and free pyridine (<5 min, $^1H$ NMR). However, in an unexpected secondary reaction the new metallacycle **10** is produced. Similar results were obtained when pyridine was added to a solution of **5** in benzene-$d_6$ (see eq 17). Traces of **3** observed during the course of the latter reaction suggest that pyridine may compete (albeit rather poorly) with phosphine for the silaacyl carbon. The small amount of **3** produced is eventually consumed as the reaction proceeds irreversibly to **10**. The set of reactions in Scheme I therefore seem plausible. The phosphine in **5** may direct pyridine coordination to the tantalum center. However, complexation of pyridine to **2** does not have the same effect, since in the presence of excess pyridine, **3** is not converted to **10**. The new metallacycle **10**, isolated as yellow crystals from preparative-scale reactions, represents (at least formally) a product derived from insertion of the silaacyl carbon atom into an ortho C–H bond of coordinated pyridine. There appears to be little, if any, primary kinetic isotope effect associated with this insertion. Thus, repeating the reaction with a 1:1 mixture of pyridine/pyridine-$d_5$ (5 equiv of each) led to isolation of **10** containing 0.50 (5) equiv of pyridine-derived protium, as measured by $^1H$ NMR.

(27) Holmes, S. J.; Schrock, R. R.; Churchill, M. R.; Wasserman, H. J. *Organometallics* **1984**, *3*, 476.
(28) Bruce, A. E.; Gambel, A. S.; Tonker, T. L.; Templeton, J. L. *Organometallics* **1987**, *6*, 1350.
(29) Belmonte, P.; Schrock, R. R.; Churchill, M. R.; Youngs, W. J. *J. Am. Chem. Soc.* **1980**, *102*, 2858.
(30) Carmona, E.; Galindo, A.; Gutiérrez-Puebla, E.; Monge, A.; Puerta, C. *Inorg. Chem.* **1986**, *25*, 3804.

**Scheme I**

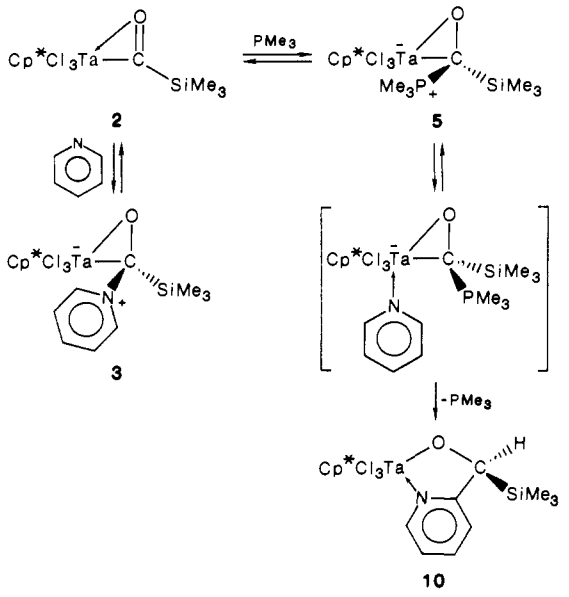

An analogous insertion reaction was observed on addition of pyridine to the $\eta^2$-silaacyl $Cp^*Cl_2Hf[\eta^2\text{-}COSi(SiMe_3)_3]$ (eq 29).[15f]

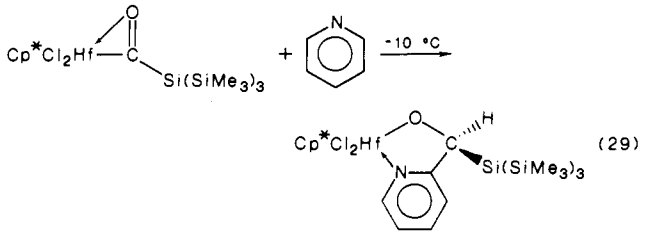

The $\eta^2$-silaacyl complex $Cp^*Cl_2Hf[\eta^2\text{-}COSi(SiMe_3)_3]$ shows no tendency to form adducts analogous to **3–7**. Recent work by Rothwell shows that reactions of this type are not limited to silaacyl systems (eq 30).[1i] Insertion of a samarium $\eta^2$-acyl into the CH bond of an aryl group has recently been observed by Evans and co-workers.[2c]

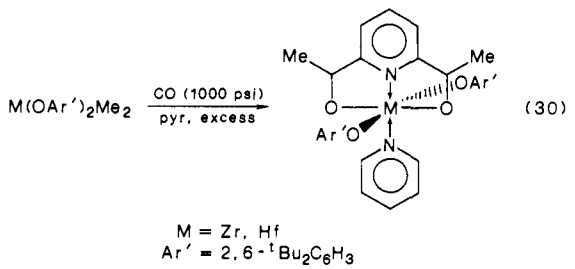

Several reactions between transition-metal hydrides and $\eta^2$-acyls have been reported.[1k,7] These reactions, such as the one shown in eq 31,[7b] lead initially to bimetallic species containing a bridging

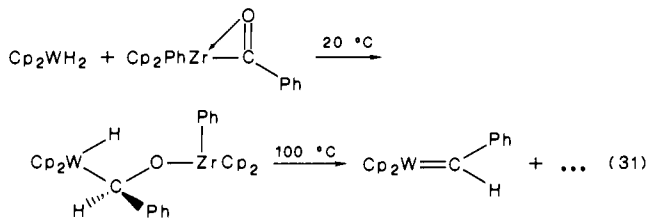

aldehyde ligand. Caulton and co-workers have suggested that these reactions involve intermolecular nucleophilic attack of a hydride ligand onto the acyl carbon.[7e] Reaction of silaacyl **2** with $Cp_2WH_2$ (eq 18) may take a similar course, initially giving the bimetallic species $Cp_2W(H)[\mu\text{-}(Me_3Si)HCO]TaCp^*Cl_3$, which undergoes subsequent rearrangements to the tungsten alkyl **11** and the tantalum oxo complex **12**. The latter reaction is quite rapid at −78 °C, and low-temperature NMR experiments provided no evidence for intermediates.

Tantalum $\eta^2$-silaacyl **2** readily undergoes carbon–carbon coupling with carbon monoxide to generate a reactive, ketene-like species. A possible mechanism for the ether-cleavage reaction is shown in Scheme II. A related process has been observed by Marks and co-workers, in which the thorium $\eta^2$-acyl $Cp^*_2Th(\eta^2\text{-}COCH_2CMe_3)Cl$ reacts with carbon monoxide to give products derived from the proposed transitory ketene $Cp^*_2Th[OC(CH_2CMe_3)=C=O]Cl$.[3a] Many examples of transition-metal ketene complexes are known,[3a,31] although none have been reported to exhibit the reactivity toward ether solvents that we report here (eq 19 and 21). Also, we are unaware of any such reactions involving organic ketenes. The ketene derivative represented by resonance hybrid structures D–F may be activated toward reaction with ethers via stabilization of resonance structures E and F by the $SiMe_3$ and tantaloxy substituents, which impart substantial electrophilic character to the ketene $\alpha$-carbon. In addition, nucleophilic attack of the ether may be aided by concurrent Ta–O bond formation to give the betaine complex G.

The accessibility of ether $\beta$-hydrogens for abstraction by the ketene $\beta$-carbon appears to be crucial in determining the outcome of the reaction. This is explained by the mechanism of Scheme II, which proposes that the ether $\beta$-hydrogen is transferred via an electrocyclic 1,5-shift. Thus, carbonylation of **1** in 2-methyltetrahydrofuran leads to the ring-opened ether-cleavage product **15** (eq 21), presumably by a process analogous to that shown in Scheme II. In contrast, the same reaction in tetrahydrofuran results only in reductive elimination of $Me_3SiCl$ to form $Cp^*TaCl_2(CO)_2(THF)$ (**16**), apparently because the $\beta$-hydrogens of tetrahydrofuran are not sterically available for abstraction in an adduct analogous to G. Therefore in the latter reaction, the reductive elimination pathway predominates. This suggests that many of the steps in Scheme II are reversible. Note that traces of tantalum carbonyl species were also observed in the diethyl ether cleavage reaction.

Zwitterionic species similar to G have been proposed as intermediates in analogous reactions in which ethers with $\beta$-hydrogens are cleaved by arynes (eq 32[32]). In these latter reactions,

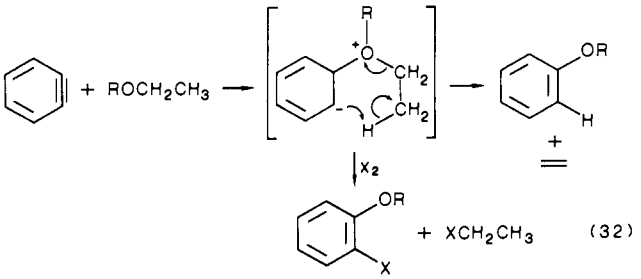

evidence for the intermediate betaine complex was obtained by trapping reactions with halogen (eq 32).[32b] In an attempt to trap the proposed intermediate G, silyl complex **1** was carbonylated in the presence of MeI (10 equiv in diethyl ether solvent). However, no evidence was obtained for the trapped product $Cp^*Cl_3Ta[OCMe(SiMe_3)COOEt]$. The isolated yield of **13** indicated that the course of reaction was not diverted significantly by the presence of MeI.

(31) See, for example: (a) Klimes, J.; Weiss, E. *Angew. Chem., Int. Ed. Engl.* **1982**, *21*, 205. (b) Herrmann, W. A.; Plank, J. *Ibid.* **1978**, *17*, 525. (c) Redhouse, A. D.; Herrmann, W. A. *Ibid.* **1976**, *15*, 615. (d) Cutler, A. R.; Bodnar, T. W. *J. Am. Chem. Soc.* **1983**, *105*, 5926.

(32) (a) Richmond, G. D.; Spendel, W. *Tetrahedron Lett.* **1973**, 4557. (b) Hayashi, S.; Ishikawa, N. *Bull. Chem. Soc. Jpn.* **1972**, 642. (c) Brewer, J. P. N.; Hearney, H.; Jablonski, J. M. *Tetrahedron Lett.* **1968**, 4455. (d) Franzen, V.; Joscheck, H. I.; Mertz, C. *Justus Liebigs Ann. Chem.* **1962**, *654*, 82. (e) Hellmann, H.; Eberle, D. *Ibid.* **1963**, *662*, 188. (f) Hoffmann, R. W. *Dehydrobenzene and Cycloalkynes*; Academic: New York, 1967. (g) Gilchrist, T. L. In *The Chemistry of Functional Groups, Part 1, Supplement C: The Chemistry of Triple-Bonded Functional Groups*; Patai, S., Rappoport, Z., Eds.; Wiley: New York, 1983; pp 405–410.

**Scheme II**

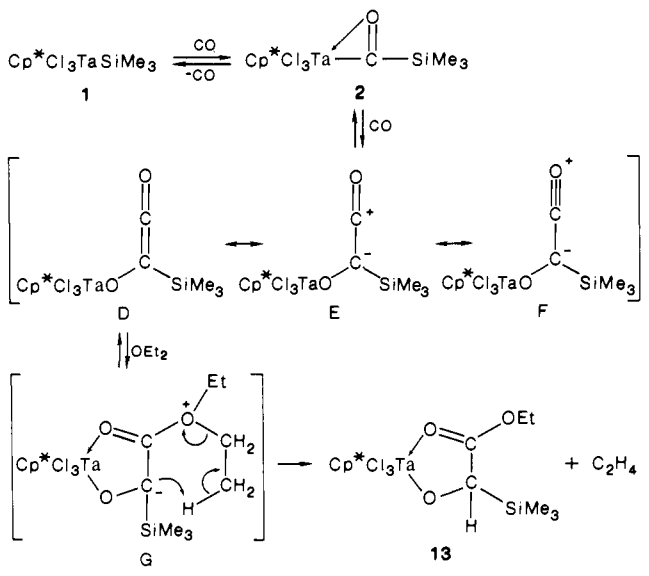


The proposed 1,5-shift of hydrogen to form products from intermediate G is similar to pyrolytic eliminations of vinyl and alkynyl ethers (eq 33[33] and 34[34]), which are examples of retroene

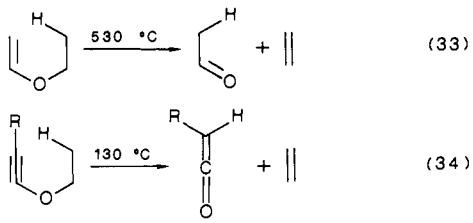


reactions.[35] These reactions are thought to proceed via a six-membered, cyclic transition state.[35] Note that additions to ketenes may occur by a stepwise, dipolar process involving zwitterionic intermediates.[36] Ketenes bearing electronegative substituents, such as $(Me_3C)(NC)C{=}C{=}O$[37] and $(CF_3)_2C{=}C{=}O$,[38] undergo ene-type reactions in which an allylic hydrogen is abstracted. These processes appear to proceed through a dipolar intermediate adduct.[37,38] In the ether-cleavage reaction we favor the stepwise process involving G, since polar reactants are involved and the tantaloxy ($Cp^*Cl_3TaO$) and $SiMe_3$ substituents are expected to increase the stability of the dipolar intermediate. For the carbonylation reaction involving diethyl ether cleavage (eq 19), the isotope effect of 1.9 (4) suggests that C–H bond breaking is involved in the rate-determining step.

Attempts to observe the ketene-like intermediate spectroscopically (by NMR or FT IR) were not successful. Therefore the structure of this reactive species is not well established. Formation of stable adducts between silaacyl **2** and Lewis bases suggests an alternative structure for a carbon–carbon coupled intermediate, the acylium ion structure H, with a tetrahedral carbon center and

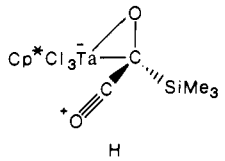


a Ta–C bond. Attack of nucleophiles onto the acylium carbon of H could occur directly or follow rupture of the Ta–C bond to give ketene D.

Further evidence for intermediacy of a ketene-like species in the carbonylation of **1** was obtained by isolation of the trapped complexes **18** and **19**. Similar processes that trap isolated[39] and transitory[3a] metal-complexed ketenes are known. It appears that once formed, the "ketene" rapidly decomposes or is intercepted by a suitable trapping agent. Similar results have been observed by Marks and co-workers, who carried out a detailed kinetic study of the carbonylation chemistry of the thorium $\eta^2$-acyl $Cp^*_2Th(\eta^2\text{-}COCH_2CMe_3)Cl$.[3a] The latter complex also appears to react with CO to form a transitory ketene species that may be trapped with $PMe_3$ or $PPh_3$. The rate of appearance of trapped product was found to be dependent upon CO concentration, but independent of both the concentration and nature of the phosphine.

The tricyclohexylphosphine derivative **19** does not serve as a source of the free ketene that is responsible for ether cleavage. Thus, no reaction was detected between **19** and 2-methyltetrahydrofuran after 2 days at 90 °C in benzene-$d_6$.

The reactivity of the neopentyl $\eta^2$-acyl $Cp^*Cl_3Ta(\eta^2\text{-}COCH_2CMe_3)$ (**21**) has been investigated in order to make comparisons with the $\eta^2$-silaacyl **2**. Some differences in reactivity between **2** and **21** are illustrated in Scheme III. Whereas **2** decomposes rapidly at room temperature, **21** is quite stable, melting at 132 °C without decomposition. Unlike **2**, the latter complex does not undergo attack at the acyl carbon by either carbon monoxide or pyridine. Rather, pyridine attacks the tantalum center of **21** to produce the thermally unstable 18-electron complex **22**. This coordination of pyridine induces a 1,2-hydrogen shift to produce the *cis*-enolate **23**. Although similar 1,2-hydrogen shifts have ample precedent in early transition and actinide metal $\eta^2$-acyl chemistry, an example of a ligand-induced 1,2-shift is somewhat unusual.[40]

## Experimental Section

Manipulations were performed under an atmosphere of nitrogen or argon using Schlenk techniques or in a Vacuum Atmospheres glovebox. Dry, oxygen-free solvents were employed throughout. Elemental analyses were performed by Galbraith or Schwarzkopf laboratories. Infrared spectra were recorded on a Perkin-Elmer 1330 spectrometer. NMR spectra were recorded with a GE-QE 300 instrument at 300, 122, or 75.5 MHz ($^1H$, $^{31}P$, and $^{13}C$, respectively), a Nicolet WB-200 (50 MHz, $^{13}C$), or a Varian EM 390 (90 MHz, $^1H$). The solid-state NMR spectra were recorded at the University of Colorado Regional NMR Center (funded by NSF Grant No. CHE-8208821) on a Nicolet NT-150 spectrometer at a frequency of 37.735 MHz ($^{13}C$) or 60.745 MHz ($^{31}P$) with a home-built cross-polarization magic-angle spinning (CP-MAS) unit, including the probe. The decoupling field was 13 G (55 kHz). The spinner system is a modified version of Wind's,[41] with a sample volume of 0.3 $cm^3$. The samples were spun at 3800 rps (100 ppm). The CP contact time was 2 ms, and the repetition time was 2 s. 2K points were collected with a spectrum width of 40 kHz and an acquisition time of 52 ms. The time-domain data were not multiplied by an exponential broadening

(33) (a) Blades, A. T.; Murphy, G. W. *J. Am. Chem. Soc.* **1952**, *74*, 1039. (b) Blades, A. T. *Can. J. Chem.* **1953**, *31*, 418. (c) McEwen, I.; Taylor, R. *J. Chem. Soc., Perkin Trans. 2* **1982**, 1179.

(34) (a) Hasek, R. H.; Gott, P. G.; Martin, J. C. *J. Org. Chem.* **1964**, *29*, 2510. (b) Nieuwenhuis, J.; Arens, J. F. *Recl. Trav. Chim. Pays-Bas* **1958**, *77*, 761.

(35) (a) Hoffmann, H. M. R. *Angew. Chem., Int. Ed. Engl.* **1969**, *8*, 556. (b) DePuy, C. H.; King, R. W. *Chem. Rev.* **1960**, *60*, 431. (c) Egger, K. W.; Vitins, P. *Int. J. Chem. Kinet.* **1974**, *6*, 429.

(36) (a) Ulrich, H. *Cycloaddition Reactions of Heterocumulenes*; Academic: New York, 1967; pp 38–109. (b) Otto, P.; Feiler, L. A.; Huisgen, R. *Angew. Chem., Int. Ed. Engl.* **1968**, *7*, 737. (c) Gompper, R. *Angew. Chem., Int. Ed. Engl.* **1969**, *8*, 312. (d) Lehr, R. E.; Marchand, A. P. in *Pericyclic Reactions*; Marchand, A. P., Lehr, R. E., Eds.; Academic: New York, 1977; Vol. I, pp 1–51. (e) Ghosez, L.; O'Donnell, M. J. In *Pericyclic Reactions*; Marchand, A. P., Lehr, R. E., Eds.; Academic: New York, 1977; Vol. II, pp 79–140. (f) Moore, H. W.; Wilbur, D. S. *J. Am. Chem. Soc.* **1978**, *100*, 6523.

(37) (a) Bampfield, H. A.; Brook, P. R. *J. Chem. Soc., Chem. Commun.* **1974**, 172. (b) Brook, P. R.; Hunt, K. *Ibid.* **1974**, 989.

(38) England, D. C.; Krespan, C. G. *J. Org. Chem.* **1970**, *35*, 3300, 3308, 3312, 3322.

(39) (a) Kreissl, F. R.; Wolfgruber, M.; Sieber, W. J. *Organometallics* **1983**, *2*, 1266. (b) Kreissl, F. R.; Wolfgruber, M.; Thewalt, U. *J. Organomet. Chem.* **1986**, *317*, 175.

(40) Beshouri, S. M.; Fanwick, P. E.; Rothwell, I. P.; Huffman, J. C. *Organometallics* **1987**, *6*, 891.

(41) Wind, R. A.; Anthonio, F. E.; Duijvestijn, M. J.; Smidt, J.; Trommel, J.; de Vette, G. M. C. *J. Magn. Reson.* **1983**, *52*, 424.

function. Chemical shifts are relative to external tetramethylsilane, with hexamethylbenzene as a secondary standard (methyl signal at 17.35 ppm). Mass spectral determinations were performed at the Midwest Center for Mass Spectrometry (an NSF regional facility, Grant No. CHE-8211164), at the U.C. Riverside Mass Spectrometry Laboratory, or at the University of Minnesota Mass Spectrometry Laboratory. GC analyses were conducted with a Varian 3400 instrument utilizing a Varian 4290 integrating recorder. A 3 m × $^1/_8$ in. stainless steel column with 25% 1,2,3-tris(2-cyanoethoxy)propane as stationary phase was employed. Carbon monoxide (Liquid Carbonics) and 90% $^{13}C$ carbon monoxide (MSD) were used as received.

Pyridine, 2,6-dimethylpyridine (DMP), and 4-methylpyridine were distilled from activated molecular sieves (4 Å) under argon. $PMe_3$, $PEt_3$, and $P(OMe)_3$ were vacuum distilled before use. $PCy_3$ was recrystallized from ethanol and dried under vacuum. Unless otherwise stated, $^{13}C$-labeled compounds were prepared by substituting $^{13}C$-enriched CO in the same procedure used to make the unlabeled derivatives.

More complete listings of infrared data are given in the Supplementary Material.

**$Cp^*Cl_3Ta(\eta^2\text{-}COSiMe_3)$ (2).** A solution of **1** (0.48 g, 0.97 mmol) in pentane (20 mL) was stirred under 1 atm of CO for 30 min. Cooling this solution to −45 °C for 8 h precipitated **2** (0.45 g, 89%) as an orange powder. The complex decomposes to a green-black tar within 30 min at 22 °C; however, at −45 °C it is stable for at least 1 week. IR (benzene-$d_6$, $CaF_2$, $cm^{-1}$): 1462 m ($\nu_{CO}$).

**$Cp^*Cl_3Ta(\eta^2\text{-}^{13}COSiMe_3)$ (2-$^{13}C$).** $^{13}CO$ (2 mL) was syringed through a rubber septum into an NMR tube containing **1** (0.020 g) in toluene-$d_8$ (0.4 mL). The color of the solution changed from green to orange as the reaction proceeded. As monitored by $^1H$ NMR, conversion of **1** to **2**-$^{13}C$ was complete in ca. 30 min. Solutions of **2**-$^{13}C$ generated by this method are stable for approximately 1 h at 22 °C. IR (toluene-$d_8$, $CaF_2$, $cm^{-1}$): 1428 m ($\nu_{CO}$).

**$Cp^*Cl_3Ta[\eta^2\text{-}OC(pyr)SiMe_3]$ (3).** After a pentane (30 mL) solution of **1** (1.56 g, 3.15 mmol) and pyridine (0.5 mL, excess) under CO (80 psi) was stirred for 10 min, the resulting orange precipitate was isolated and washed with pentane (20 mL). Crystallization from toluene (50 mL) yielded orange crystals (mp 95–98 °C) in 92% yield (1.75 g). Anal. Calcd for $C_{19}H_{29}Cl_3NOSiTa$: C, 37.9; H, 4.85; Cl, 17.6. Found: C, 38.0; H, 4.60; Cl, 17.0.

**$Cp^*Cl_3Ta[\eta^2\text{-}OC(DMP)SiMe_3]$ (4).** The synthetic method for **3** was used, giving **4** as an orange solid (0.34 g, 90%) after washing with pentane.

**$Cp^*Cl_3Ta[\eta^2\text{-}OC(PMe_3)SiMe_3]$ (5).** A pentane solution (40 mL) of **1** (0.82 g, 1.7 mmol) and $PMe_3$ (0.3 mL, excess) was pressurized with CO and stirred for 10 min. The resulting orange precipitate was isolated by filtration, washed with pentane (10 mL), and dried under vacuum (yield 0.89 g, 90%). Compound **5** forms dark blue solutions in benzene-$d_6$ and diethyl ether, which are stable for ca. 2 h at 22 °C. Attempts at recrystallization in diethyl ether or toluene were frustrated by decomposition.

**$Cp^*Cl_3Ta[\eta^2\text{-}OC(PEt_3)SiMe_3]$ (6).** (a) Following the method for **5** above, **1** (1.00 g, 2.02 mmol) and $PEt_3$ (0.24 g, 2.0 mmol) in pentane (50 mL) yielded **6** as an orange powder in 85% yield (1.10 g).

(b) An unstirred solution of **1** (0.30 g, 0.60 mmol) and $PEt_3$ (0.30 mL, excess) in pentane (30 mL) was allowed to stand under a blanket of CO (10 psi). After 12 h, large red crystals (mp 150–153 °C) suitable for X-ray diffraction were isolated by filtration (0.25 g, 65%). As with **5**, solutions of **6** were unstable, and repeated attempts at recrystallization were unsuccessful. Anal. Calcd for $C_{20}H_{39}Cl_3OPTaSi$: C, 37.4; H, 6.12; Cl, 16.6. Found: C, 36.0; H, 6.32; Cl, 15.9.

**$Cp^*Cl_3Ta[OC(SiMe_3)NNCPh_2]$ (8).** A solution of violet $Ph_2CN_2$ (0.24 g, 1.2 mmol) in benzene (10 mL) was added to a solution of **2** (0.60 g, 1.2 mmol) in benzene (20 mL). After stirring for 10 min, the orange solution was evaporated and the oily residue extracted with diethyl ether (30 mL). Filtration followed by concentration to ca. 5 mL and cooling to −45 °C overnight afforded yellow crystals of **8** (mp 190–192 °C) in 57% yield (0.49 g). Anal. Calcd for $C_{27}H_{34}Cl_3N_2OSiTa$: C, 45.2; H, 4.77; Cl, 14.8; N, 3.90. Found: C, 45.3; H, 4.75; Cl, 14.3; N, 3.76.

A solution of $Ph_2CN_2$ (0.008 g, 0.04 mmol) in benzene-$d_6$ (0.2 mL) was added via syringe to a septum-sealed NMR tube containing a solution of **2**-$^{13}C$ (0.02 g, 0.04 mmol) in benzene-$d_6$. In addition to peaks due to **8**-$^{13}C$, the following signals were recorded: $^1H$ NMR: $\delta$ 0.28 (d, $^3J_{CH}$ = 3 Hz, 9 H, $SiMe_3$), 2.12 (s, 15 H, $C_5Me_5$), 7.00–7.80 (m, 10 H, Ph). $^{13}C\{^1H\}$ NMR: $\delta$ 195.9 ($^{13}C(SiMe_3)$).

**$Cp^*Cl_3Ta[\eta^2\text{-}OC(4\text{-}Me\text{-}pyr)SiMe_3]$ (9).** The method used to prepare **3** was followed using **1** (0.50 g, 1.0 mmol) and 4-methylpyridine (0.2 mL, excess) in pentane (30 mL). Recrystallization of the resulting orange precipitate from toluene afforded 0.55 g (89%) of **8** as orange crystals.

**$Cp^*Cl_3Ta[OCH(SiMe_3)\text{-}o\text{-}C_5H_4N]$ (10).** A benzene solution (10 mL) of **5** (0.50 g, 0.83 mmol) and pyridine (0.13 mL, excess) was stirred for 1 day. After removal of volatiles, the brown residue was extracted with diethyl ether (3 × 20 mL), the combined extracts were cooled to −45 °C for 8 h, and the product **10** was isolated as yellow crystals (mp 165–167 °C) in 78% yield (0.39 g). Anal. Calcd for $C_{19}H_{29}Cl_3ONSiTa$: C, 37.9; H, 4.85; Cl, 17.6. Found: C, 38.0; H, 5.15; Cl, 17.5. Mass spectrum: 590.0256 (M − $CH_3$, with correct isotope envelope).

**Carbonylation of 1 in the Presence of $Cp_2WH_2$.** (a) A solution of **1** (0.30 g, 0.60 mmol) and $Cp_2WH_2$ (0.19 g, 0.60 mmol) in benzene (30 mL) was stirred for 30 min under a CO atmosphere (50 psi). The orange solution was evaporated under reduced pressure, and the residue was extracted with diethyl ether (2 × 20 mL). These extracts were concentrated to ca. 20 mL and cooled to −45 °C for 8 h to yield **11** as red crystals (mp 194–195 °C) in 76% yield (0.20 g). The yellow residue remaining in the reaction flask was extracted into toluene (30 mL). Concentration to ca. 10 mL followed by cooling to −45 °C gave **12** as a yellow powder (mp >300 °C) in 63% yield (0.15 g).

(b) A less convenient procedure, in which $Cp_2WH_2$ was added to a freshly prepared solution of **2**, gave similar results.

**$Cp_2W(CH_2SiMe_3)Cl$ (11).** Anal. Calcd for $C_{19}H_{21}ClSiW$: C, 38.5; H, 4.85; Cl, 8.12. Found: C, 38.3; H, 4.82; Cl, 8.54. Mass spectrum calcd for $^{12}C_{14}H_{21}{}^{35}Cl^{28}Si^{184}W$: 436.06106. Found: 436.06009 (FABS, ONPOE).

**$[Cp^*Cl_2TaO]_n$ (12).** Anal. Calcd for $C_{10}H_{15}Cl_2OTa$: C, 29.8; H, 3.75; Cl, 17.6. Found: C, 29.2; H, 3.90; Cl, 16.9.

**Reaction of 11 with HCl.** Dry HCl gas (0.70 mL, 0.028 mmol) was syringed into a solution of **11** (0.012 g, 0.028 mmol) in benzene-$d_6$ (0.4 mL). A colorless solution and a blue-green precipitate quickly developed. Analysis of the volatile components revealed the presence of $SiMe_4$ as the sole $SiMe_3$-containing product (by $^1H$ NMR and GC). The IR spectrum of the precipitate was identical with that of an authentic sample of $Cp_2WCl_2$.

**$Cp^*Cl_3Ta[OCH(SiMe_3)C(O)OEt]$ (13).** A solution of **1** (2.00 g, 4.03 mmol) in diethyl ether (50 mL) was stirred for 2 h under a CO atmosphere (50 psi). The resulting orange solution was filtered and the volume was reduced to ca. 25 mL in vacuo. Cooling to −45 °C overnight gave 0.93 g of yellow-orange **13** (mp 130–133 °C, 39%). Compound **13** may be further purified by recrystallization from diethyl ether or by sublimation (120 °C, $10^{-3}$ mmHg). Anal. Calcd for $C_{17}H_{30}Cl_3O_3SiTa$: C, 34.2; H, 5.05; Cl, 17.8. Found: C, 34.1; H, 4.91; Cl, 18.1. IR (Nujol mull, CsI, $cm^{-1}$): 1610 vs ($\nu_{C=O}$). Mass spectrum (EI): 560.0749 (M − HCl).

**13-$^{13}C_2$.** IR (Nujol mull, CsI, $cm^{-1}$): 1578 vs ($\nu_{C=O}$).

**$LiOCH_2CO_2Et$.** BuLi (30 mL of a 1.6 M hexane solution) was added dropwise to a solution of $HOCH_2CO_2Et$ (5.0 g, 48 mmol) in pentane (50 mL). After 2 h of stirring at room temperature, volatiles were removed from the white suspension. The solid residue was washed several times with pentane (3 × 50 mL) and dried in vacuo (3.9 g, 74%).

**$Cp^*Cl_3Ta[OCH_2C(O)OEt]$ (14). (a) From 13.** Tetrahydrofuran (20 mL, −78 °C) was added to a flask containing **13** (0.33 g, 0.55 mmol) and $KOSiMe_3$ (0.071 g, 0.55 mmol) at −78 °C. The solution was allowed to warm to room temperature with stirring, and the volatiles were removed in vacuo. Extraction with diethyl ether (30 mL) followed by concentration to 10 mL and cooling to −45 °C gave yellow crystals of **14** in 42% yield (0.12 g, mp 195–200 °C).

**(b) From $Cp^*TaCl_4$ and $LiOCH_2CO_2Et$.** Tetrahydrofuran (50 mL) was added to a mixture of $Cp^*TaCl_4$ (2.00 g, 4.38 mmol) and $LiOCH_2CO_2Et$ (0.48 g, 4.4 mmol). After stirring at room temperature overnight, the mixture was worked up as in (a) to afford 1.15 g (50%) of yellow, crystalline **14**.

Spectroscopic properties of the products from both preparations were identical ($^1H$ and $^{13}C$ NMR, IR). Mixture melting point of product from (a) and (b): 196–198 °C. Anal. Calcd for $C_{14}H_{22}Cl_3O_3Ta$: C, 32.0; H, 4.22; Cl, 20.2. Found: C, 33.2; H, 3.66; Cl, 19.8. Molecular weight calcd: 526. Found: 560 (isothermal distillation).

**$Cp^*Cl_3Ta[OCH(SiMe_3)C(O)O(CH_2)_3CH{=}CH_2]$ (15).** After stirring under a CO atmosphere (100 psi) for 20 min, a solution of **1** (0.46 g, 0.93 mmol) in 2-methyltetrahydrofuran (10 mL) was evaporated under a dynamic vacuum. Following extraction with diethyl ether (2 × 15 mL), the orange solution was concentrated (15 mL) and cooled to −15 °C overnight. Compound **15** was isolated by filtration as an orange powder (mp 134–136 °C) in 66% yield (0.39 g). Anal. Calcd for $C_{20}H_{34}Cl_3O_3SiTa$: C, 37.7; H, 5.37; Cl, 16.7. Found: C, 37.2; H, 5.12; Cl, 16.5. Molecular weight calcd: 638. Found: 574 (isothermal distillation).

**$Cp^*Cl_2Ta(CO)_2(THF)$ (16).** A solution of **1** (0.50 g, 1.0 mmol) in tetrahydrofuran (20 mL) was pressurized with CO (50 psi) and stirred for 8 h. The resulting dark red solution was concentrated (10 mL) and cooled to −45 °C for 8 h to give orange crystals of **16** (0.20 g, 39%), mp

**Scheme III**

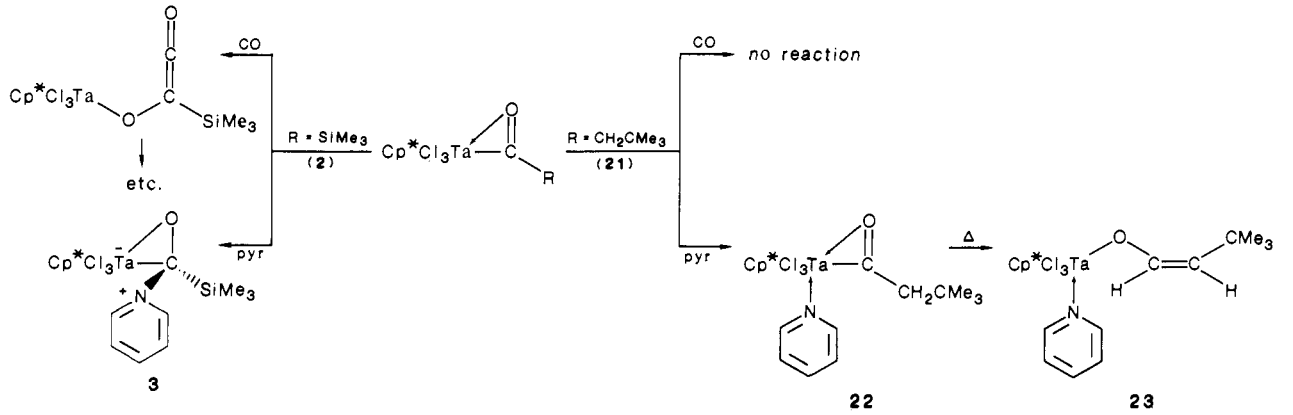


**Table V.** Crystal, Data Collection, and Refinement Parameters for **3**, **6**, and **19**

| | **3** | **6** | **19** |
|---|---|---|---|
| | (a) Crystal Parameters | | |
| formula | $C_{19}H_{29}Cl_3NOSiTa$ | $C_{20}H_{45}Cl_3OPSiTa$ | $C_{33}H_{57}Cl_3O_2PSiTa$ |
| cryst system | monoclinic | orthorhombic | monoclinic |
| space group | $P2_1/n$ | *Pcam* | $P2_1/n$ |
| *a*, Å | 10.322 (2) | 15.820 (4) | 14.751 (2) |
| *b*, Å | 14.503 (3) | 11.314 (4) | 16.294 (3) |
| *c*, Å | 16.289 (3) | 14.809 (5) | 16.378 (4) |
| $\beta$, deg | 101.73 (1) | | 105.81 (2) |
| *V*, Å$^3$ | 2392.2 (7) | 2651 (1) | 3787 (1) |
| *Z* | 4 | 4 | 4 |
| $\rho$(calcd), g cm$^{-3}$ | 1.67 | 1.36 | 1.46 |
| temp, °C | 23 | 23 | 20 |
| $\mu$, cm$^{-1}$ (Mo K$\alpha$) | 52.5 | 44.8 | 31.8 |
| cryst dimens, mm | 0.23 × 0.23 × 0.23 | 0.38 × 0.38 × 0.38 | 0.30 × 0.25 × 0.20 |
| | (b) Data Collection | | |
| diffractometer | Nicolet R3m/$\mu$ | Nicolet R3m/$\mu$ | Enraf-Nonius CAD-4 |
| radiation | Mo K$\alpha$ ($\lambda$ = 0.71073 Å) | | |
| monochromator | graphite | | |
| scan technique | Wyckoff | $\omega$ | $\theta/2\theta$ |
| $2\theta$ scan range, deg | 4° ≤ $2\theta$ ≤ 48° | 4° ≤ $2\theta$ ≤ 55° | 3° ≤ $2\theta$ ≤ 48° |
| data collected | $+h,+k,+l$ | $+h,+k,+l$ | $+h,+k,\pm l$ |
| scan speed, deg/min | variable, 5–20 | variable, 5–20 | variable, 2–10 |
| rflns collected | 4064 | 3430 | 6410 |
| independent data | 3739 | 3157 | 4344 |
| independent data obsd | 3029 ($5\sigma(F_o)$) | 2509 ($5\sigma(F_o)$) | 3834 ($3\sigma(I)$) |
| std reflns | 3 std/197 rflns | 3 std/197 rflns | 3 std/0.5 h |
| decay | ≤1% | ≤1% | ≤1% |
| | (c) Refinement | | |
| $R_F$, % | 2.62 | 6.77 | 6.41 |
| $R_{wF}$, % | 2.72 | 8.06 | 7.48 |
| $\Delta(\rho)$, e Å$^{-3}$ | 0.54 | 1.67 | 1.08 |
| $\Delta/\sigma$ | 0.06 | 0.017 | 0.025 |
| GOF | 1.297 | 1.547 | |
| data/param | 11.9 | 14.3 | 10.4 |
| weighting factor, $g^a$ | 0.001 | 0.005 | |

$^a w^{-1} = \sigma^2(F_o) + gF_o^2$.

115–118 °C dec. Anal. Calcd for $C_{16}H_{23}Cl_2O_3Ta$: C, 37.3; H, 4.50; Cl, 13.8. Found: C, 37.5; H, 4.46; Cl, 14.2. IR (benzene-$d_6$, $CaF_2$, cm$^{-1}$): 2001 vs, 1930 vs, 1917 vs. Substantial amounts of $Me_3SiCl$ were detected ($^1$H NMR, GC/MS) in the volatiles from the above reaction. No other $SiMe_3$-containing species were observed ($^1$H NMR).

**$Cp^*Cl_2Ta(CO)_2(PMe_3)$ (17).** $PMe_3$ (0.1 mL, 1 mmol) was added via syringe to a stirred suspension of **16** (0.20 g, 0.38 mmol) in benzene (10 mL). After 10 min, the dark purple solution was evaporated and the residue was dissolved in diethyl ether (20 mL). The volume of solvent was reduced to 15 mL and the solution was cooled to −45 °C for 8 h to produce purple crystals (mp 140–145 °C dec) of **17** in 89% yield (0.18 g). Anal. Calcd for $C_{15}H_{24}Cl_2O_2PTa$: C, 34.7; H, 4.66; Cl, 13.7. Found: C, 35.0; H, 4.73; Cl, 13.4.

**$Cp^*Cl_3\overline{Ta[OC(SiMe_3)C(DMP)O]}$ (18).** A solution of **1** (0.70 g, 1.4 mmol) and DMP (0.16 mL, 1.4 mmol) in toluene (15 mL) was pressurized with CO (100 psi) and stirred for 8 h. Cooling of the resulting dark red solution to −45 °C for 12 h gave 0.73 g of red crystalline **18** (78%, mp 245–250 °C dec). Anal. Calcd for $C_{22}H_{35}Cl_3NO_2TaSi$: C, 40.0; H, 5.34; Cl, 16.1. Found: C, 39.9; H, 5.39; Cl, 15.1.

**$Cp^*Cl_3\overline{Ta[OC(SiMe_3)C(PCy_3)O]}$ (19).** A solution of **1** (0.50 g, 1.0 mmol), $PCy_3$ (0.28 g, 1.0 mmol), and pentane (30 mL) was stirred at room temperature under CO (50 psi). After 2 h, volatile components were removed under dynamic vacuum, and the orange residue was extracted with toluene (2 × 15 mL). Concentration in vacuo to ca. 10 mL followed by addition of pentane (10 mL) and cooling to −45 °C overnight gave 0.44 g of dark red crystalline **19** (mp 230–235 °C dec, 54%). Anal. Calcd for $C_{33}H_{57}Cl_3O_2PSiTa$: C, 47.6; H, 6.90; Cl, 12.8. Found: C, 47.9; H, 7.22; Cl, 12.8.

**$Cp^*Cl_3TaCH_2CMe_3$ (20).** A solution of $Me_3CCH_2MgCl$ (4.9 mL of a 1.8 M solution in diethyl ether, 8.8 mmol) was added to a stirred suspension of $Cp^*TaCl_4$ (4.00 g, 8.73 mmol) in benzene (60 mL). After 4 h the volatiles were removed, and the orange residue was extracted with diethyl ether (3 × 60 mL). Concentration (to ca. 10 mL) and cooling (−45 °C) overnight produced orange crystals, 2.30 g (54%). Spectroscopic properties of the material prepared by this method were identical with those described in the original report of this complex.[20]

**$Cp^*Cl_3Ta(\eta^2\text{-}COCH_2CMe_3)$ (21).** A pentane solution of **20** (0.40 g, 0.78 mmol in 60 mL) was pressurized with CO (80 psi). After stirring

for 1 h, the orange solution was filtered, concentrated (to ca. 5 mL), and cooled to −45 °C. Orange-red crystals were isolated by filtration after 8 h (0.31 g, 76%, mp 132–133 °C). Anal. Calcd for $C_{16}H_{26}Cl_3OTa$: C, 36.8; H, 5.02; Cl, 20.4. Found: C, 36.8; H, 5.24; Cl, 20.2.

**Cp*Cl$_3$Ta(*cis*-OCH=CHCMe$_3$)(pyr) (23).** Pyridine (0.04 mL, 0.50 mmol) was added to a stirred solution of **21** (0.27 g, 0.50 mmol) in benzene (20 mL). After 10 min, the solution was evaporated under dynamic vacuum and the residue was extracted with pentane (50 mL). The volume of solvent was reduced to 5 mL, and the solution was cooled to −45 °C. Orange crystals (mp 119–120 °C) were isolated by filtration (0.21 g, 70%).

**Reaction of 21 with Pyridine at −65 °C.** Pyridine (0.003 mL, 0.04 mmol) was added to a cold (−78 °C) solution of **21**-$^{13}C$ (0.02 g, 0.04 mmol) in toluene-$d_8$ (0.4 mL). Examination by NMR ($^1$H, $^{13}$C) revealed complete conversion to a new product, **22**-$^{13}C$ (see Table I). When the probe temperature was raised to ca. −10 °C, signals due to **22**-$^{13}C$ began to disappear as a new complex was formed. Conversion was complete within 30 min at this temperature. NMR spectra of the final product in this reaction were identical with those of **23**-$^{13}C$, prepared as above.

**Single-Crystal X-ray Diffraction Studies of 3, 6, and 19.** The parameters used during the collection of diffraction data for **3**, **6**, and **19** are summarized in Table V. The crystal structures of **3** and **6** were determined at the University of Delaware; the structure of **19** was determined at The University of Texas. The crystals were mounted in thin-walled glass capillaries in an inert-atmosphere glovebox, and the capillaries were flame-sealed.

An orange crystal of **3** was found from photographic evidence and systematic absences to be uniquely assignable to the monoclinic space group $P2_1/n$. The unit-cell parameters were obtained from the angular settings of 25 reflections ($21° \leq 2\theta \leq 27°$). The data were empirically corrected for absorption (max/min transmission = 0.295/0.230) by a procedure that employs six refined parameters to define a pseudoellipsoid.

The structure was solved by heavy-atom procedures and completed by subsequent difference Fourier syntheses. All non-hydrogen atoms were anisotropically refined, and hydrogen atoms were incorporated as idealized, updated isotropic contributions ($d$(CH) = 0.96 Å) except for the pyridine hydrogen atoms, which were found and refined. All computer programs are contained in the SHELXTL (5.1) library (G. Sheldrick, Nicolet XRD, Madison, WI).

An orange-brown cube-shaped crystal of **6** was, from systematic absences and photographic evidence, found to crystallize in either of the orthorhombic space groups $Pca2_1$ or $Pcam$. $Pcam$ was initially chosen based on $E$ statistics and subsequently proved correct by the solution and refinement of the structure. No relief from the disorder described below was found on attempted refinement in $Pca2_1$. Unit-cell dimensions were obtained as for **3**. A profile fitting procedure was applied to all intensity data to improve the precision of the measurement of weak reflections. Intensity data were corrected for absorption as described for **3**.

The structure was solved by using the direct-methods program SOLV, which located the Ta atom. The remaining atoms were located from subsequent difference Fourier syntheses and a considerable amount of trial-and-error modeling of the disorder. All atoms except for $C_5Me_5$ carbon atoms were refined anisotropically. Hydrogen atoms were omitted. The asymmetric unit consists of two half-occupancy molecules intertwined about a mirror plane. Ta, Cl(1), and C(18) reside on the mirror plane and belong to both half-occupancy molecules. The C(12) atom position is at full occupancy and is also shared by both half-occupancy molecules. The Cp* carbon–carbon distances were constrained to 1.42 (2) Å. Many artifacts of the disorder are apparent in the bond metrics given in Table III: closely adjacent atomic positions are inadequately resolved, and caution is advised in the interpretation of differences in chemically related parameters. An inspection of $F_o$ vs $F_c$ values and trends based on sin $\theta$, Miller index or parity group failed to reveal any systematic errors in the data. All computer programs were those used for **3**.

For **19**, systematic absences were consistent with space group $P2_1/n$. Automatic peak search and indexing procedures yielded the monoclinic reduced primitive cell. Inspection of the Niggli values[42] revealed no conventional cells of higher symmetry. The raw intensity data were converted to structure factor amplitudes and their esd's by correction for scan speed, background, and Lorentz and polarization effects.[43,44] An empirical correction for absorption, based on the azimuthal scan data, was applied to the intensities. The structure of **19** was solved and refined by using the Enraf-Nonius "SDP-PLUS" crystallographic package (B. A. Frenz and Associates, Inc., College Station, TX 77840, 4th ed., 1981). Direct methods (MULTAN) were used, with successive cycles of difference Fourier maps followed by least-squares refinement. Data with intensities less than $3.0\sigma(I)$ and (sin $\theta$)/$\lambda$ less than 0.10 were excluded, and a non-Poisson contribution weighting scheme with an experimental instability factor of $P = 0.06$ was used in the final stages of refinement.[45] Hydrogen atoms were not located. Inspection of the residuals ordered in ranges of (sin $\theta$)/$\lambda$, $|F_o|$, and parity and value of the individual indexes showed no unusual features or trends.

**Acknowledgment** is made to the Air Force Office of Scientific Research, Air Force Systems Command, USAF, for support of this work under Grant No. AFOSR-85-0228. T.D.T. thanks the Alfred P. Sloan Foundation for a research fellowship (1988–1990).

**Registry No. 1**, 98688-32-5; **2**, 98688-38-1; **2**-$^{13}C$, 98688-39-2; **3**, 103533-63-7; **3**-$^{13}C$, 117120-29-3; **4**, 117120-10-2; **4**-$^{13}C$, 117120-30-6; **5**, 103533-64-8; **5**-$^{13}C$, 117120-11-3; **6**, 103533-65-9; **6**-$^{13}C$, 117120-12-4; **7**, 103533-66-0; **7**-$^{13}C$, 117201-58-8; **8**, 113989-38-1; **8**-$^{13}C$, 117144-67-9; **9**, 117120-21-5; **10**, 117120-22-6; **10**-$^{13}C$, 117120-13-5; **10**-$^{13}C$-$d_5$, 117120-14-6; **11**, 117120-23-7; **11**-$^{13}C$, 117120-15-7; **12**, 117120-24-8; **13**, 98688-33-6; **13**-$^{13}C_2$, 98688-37-0; **14**, 98688-34-7; **15**, 98688-36-9; **16**, 98688-40-5; **17**, 117120-25-9; **18**, 117120-32-8; **18**-$^{13}C_2$, 117120-16-8; **19**, 117120-31-7; **19**-$^{13}C_2$, 117120-17-9; **20**, 68087-41-2; **21**, 117120-26-0; **21**-$^{13}C$, 117120-18-0; **22**, 117120-20-4; **22**-$^{13}C$, 117120-27-1; **23**, 117120-28-2; **23**-$^{13}C$, 117120-19-1; $Ph_2CN_2$, 15409-32-2; $Cp_2WH_2$, 1271-33-6; $Cp_2WCl_2$, 12184-26-8; $LiOCH_2CO_2Et$, 98688-35-8; $HOCH_2CO_2Et$, 623-50-7; Cp*$TaCl_4$, 71414-47-6; $Me_3CCH_2MgCl$, 13132-23-5.

**Supplementary Material Available:** A listing of infrared data for new compounds, tables of atomic coordinates for **3**, **6**, and **19**, tables of anisotropic thermal parameters for **3**, **6**, and **19**, listings of more bond length and angle data for **3**, **6**, and **19**, and a table of hydrogen atom coordinates for **3** (20 pages); a listing of observed and calculated structure factors for **3**, **6**, and **19** (53 pages). Ordering information is given on any current masthead page.

(42) Roof, R. B., Jr. *A Theoretical Extension of the Reduced-Cell Concept in Crystallography*, Publication LA-4083; Los Alamos Scientific Laboratory: Los Alamos, NM, 1969.

(43) *Structure Determination Package User's Guide*; B. A. Frenz and Associates: College Station, TX, 1982.

(44) The data reduction formulas are $F_o^2 = (w/Lp)(C - 2B)$, $\sigma_o(F_o^2) = (w/LP)(C + 4B)^{1/2}$, $F_o = (F_o^2)^{1/2}$, and $\sigma_o(F) = \sigma_o(F_o^2)/2F_o$.

(45) $P$ is used in the calculation of $\sigma(I)$ to downweight intense reflections in the least-squares refinement. The function minimized was $\sum w(|F_o| - |F_c|)^2$, where $w = 4(F_o)^2/[\sum(F_o)^2]^2$. $[\sum(F_o)^2]^2 = [S^2(C + R^2B) + [P(F_o)^2]^2]/(Lp)^2$, where $S$ is the scan rate, $C$ is the total integrated peak count, $R$ is the ratio of scan time to background counting time, $B$ is the total background count, and $Lp$ is the Lorentz–polarization factor.